



Age-associated insolubility of parkin in human midbrain is linked to redox balance and sequestration of reactive dopamine metabolites

Jacqueline M. Tokarew^{1,2} · Daniel N. El-Kodsi^{1,2} · Nathalie A. Lengacher^{1,2} · Travis K. Fehr^{1,2} · Angela P. Nguyen¹ · Bojan Shutinoski¹ · Brian O’Nuallain³ · Ming Jin³ · Jasmine M. Khan¹ · Andy C. H. Ng¹ · Juan Li¹ · Qiubo Jiang¹ · Mei Zhang⁴ · Liqun Wang³ · Rajib Sengupta^{5,6} · Kathryn R. Barber⁷ · An Tran⁷ · Doo Soon Im^{20,21} · Steve Callaghan²⁰ · David S. Park^{20,21} · Stephanie Zandee⁸ · Xiajun Dong⁹ · Clemens R. Scherzer⁹ · Alexandre Prat⁸ · Eve C. Tsai^{1,10} · Masashi Takashi¹¹ · Nobutaka Hattori¹¹ · Jennifer A. Chan¹² · Luigi Zecca¹³ · Andrew B. West^{14,15} · Arne Holmgren⁵ · Lawrence Puente¹⁶ · Gary S. Shaw⁷ · Gergely Toth¹⁷ · John M. Woulfe^{1,4} · Peggy Taylor³ · Julianna J. Tomlinson^{1,18} · Michael G. Schlossmacher^{1,18,19}

Received: 20 November 2020 / Revised: 11 January 2021 / Accepted: 13 January 2021 / Published online: 10 March 2021
© The Author(s) 2021

Abstract

The mechanisms by which parkin protects the adult human brain from Parkinson disease remain incompletely understood. We hypothesized that parkin cysteines participate in redox reactions and that these are reflected in its posttranslational modifications. We found that in *post mortem* human brain, including in the *Substantia nigra*, parkin is largely insoluble after age 40 years; this transition is linked to its oxidation, such as at residues Cys95 and Cys253. In mice, oxidative stress induces posttranslational modifications of parkin cysteines that lower its solubility *in vivo*. Similarly, oxidation of recombinant parkin by hydrogen peroxide (H₂O₂) promotes its insolubility and aggregate formation, and in exchange leads to the reduction of H₂O₂. This thiol-based redox activity is diminished by parkin point mutants, e.g., p.C431F and p.G328E. In *prkn*-null mice, H₂O₂ levels are increased under oxidative stress conditions, such as acutely by 1-methyl-4-phenyl-1,2,3,6-tetrahydropyridine toxin exposure or chronically due to a second, genetic hit; H₂O₂ levels are also significantly increased in parkin-deficient human brain. In dopamine toxicity studies, wild-type parkin, but not disease-linked mutants, protects human dopaminergic cells, in part through lowering H₂O₂. Parkin also neutralizes reactive, electrophilic dopamine metabolites via adduct formation, which occurs foremost at the primate-specific residue Cys95. Further, wild-type but not p.C95A-mutant parkin augments melanin formation *in vitro*. By probing sections of adult, human midbrain from control individuals with epitope-mapped, monoclonal antibodies, we found specific and robust parkin reactivity that co-localizes with neuromelanin pigment, frequently within LAMP-3/CD63⁺ lysosomes. We conclude that oxidative modifications of parkin cysteines are associated with protective outcomes, which include the reduction of H₂O₂, conjugation of reactive dopamine metabolites, sequestration of radicals within insoluble aggregates, and increased melanin formation. The loss of these complementary redox effects may augment oxidative stress during ageing in dopamine-producing cells of mutant *PRKN* allele carriers, thereby enhancing the risk of Parkinson’s-linked neurodegeneration.

Dedication: This work is dedicated to the memories of Mr. Bruce Hayter (1962–2019), a tireless advocate for persons with young-onset parkinsonism, and our co-author, Dr. Arne Holmgren (1940–2020), a pioneer in redox biology. We are grateful to Dr. Oleh Hornykiewicz (1927–2020), a leader in the pursuit of biochemical investigations of the human brain, for his encouragement.

Jacqueline M. Tokarew and Daniel N. El-Kodsi have contributed equally to this work.

Arne Holmgren: Deceased.

Extended author information available on the last page of the article

Keywords Young-onset Parkinson disease · Parkinsonism · Parkin · *PRKN/PARK2* gene · Redox chemistry · Dopamine metabolism · Neuromelanin · Anti-oxidant

Introduction

Bi-allelic mutations in *PRKN*, which encodes parkin, lead to a young-onset, recessive form of Parkinson disease (PD) [39, 42]. Pathology studies of parkin-deficient brains have demonstrated that neuronal loss is largely restricted to the *S. nigra* and *L. coeruleus*, two brainstem nuclei that synthesize dopamine (reviewed in Doherty et al. [15]).

Parkin is a principally cytosolic protein. It has been associated with diverse cellular functions, foremost related to its ubiquitin ligase (E3) activity, the control of inflammation signalling, and maintenance of mitochondrial integrity, as mediated through participation in mitophagy and mitochondrial antigen presentation (MITAP) [5, 57–59, 63, 65, 67, 88] (reviewed in Barodia et al. [4]). Although mitophagy has recently been shown to be co-regulated by parkin in the developing heart of mice [26], the diverse roles ascribed to parkin function have not yet explained its selective neuroprotection. For example, vertebrate models of genomic *prkn* deletion do not reproduce dopamine cell loss; one exception is the parkin-deficient *Polg* mouse, where mitochondrial DNA mutagenic stress had been added as a second, genetic hit [75]. The general lack of dopamine cell loss in genomic parkin deficiency-based models of vertebrates could be due to compensatory mechanisms [86], a shorter life span of non-human mammals, and possibly, unique aspects of dopamine metabolism in humans. The latter is exemplified by the generation of cytoplasmic neuromelanin in dopamine synthesizing neurons beginning after childhood [110]. Nevertheless, genomic *prkn*-null models have revealed biochemical and structural changes in high energy-producing cells of flies and murine tissues [4, 21, 102], which suggested the presence of elevated oxidative stress [34, 70, 74]. These observations pointed at a contribution of parkin to redox homeostasis in vivo.

Redox equilibrium invariably involves cysteine-based chemistry. There, thiols are subjected to oxidative modifications by reactive oxygen-, reactive nitrogen- and reactive electrophilic species (ROS, RNS, RES) [2, 52], some of which are reversible. Proteins irreversibly conjugated by RES, including by electrophilic dopamine radicals, are either degraded or sequestered within inclusions. It is thought that the latter process occurs via lysosomal functions and underlies neuromelanin formation throughout adulthood [83].

Human parkin contains 35 cysteines [42], its murine homologue 34. Of these, 28 cysteines are involved in the chelation of eight zinc ions within four RING domains [31]. Although Cys431 has been identified as critical in catalyzing human parkin's E3 ligase activity, 6 other cysteines are

structurally unaccounted for, including Cys95 located within parkin's 'linker' domain. Several reports have demonstrated the unique sensitivity of parkin to ROS and RES in cells [50, 60, 103]. Further, RNS and sulfhydration can also modify its cysteines, and NO-/NO₂-modified parkin variants have been described in cells and brain tissue [6–8, 97, 107]. Oxidation of parkin has been linked to both activating ('gain-of-function') and detrimental ('loss-of-function') outcomes when tested in the context of parkin's E3 ligase activity in vitro [8, 51, 60, 107].

We found that wild-type parkin is highly oxidized and insoluble in adult human midbrain, leading us to explore non-E3 ligase-mediated, protective functions. Owing to its large number of cysteine-based thiols, we hypothesized: one, that parkin confers neuroprotection by acting as an anti-oxidant molecule in vivo and thereby contributes to redox balance; two, specifically, that parkin directly lowers ROS- as well as RNS-linked stressors and promotes the conjugation of dopamine radicals (RES); and three, we posited that selective neurodegeneration in *PRKN*-linked, autosomal-recessive PD (ARPD) could be partially explained by the absence of parkin-mediated sequestration of toxic metabolites during decades of human ageing.

Materials and methods

Tissue collection

All tissues were collected in accordance with Institutional Review Board-approved guidelines. Fresh frozen samples of the cortical human brain from subjects under 50 years of age were acquired through the University of Alabama and the Autism Tissue Program. *Post mortem*, frozen brain samples from frontal cortices were also obtained from the NICHD Brain and Tissue Bank at the University of Maryland. Brain tissues, including midbrain specimens, with short *post mortem* interval (PMI) were obtained from patients diagnosed clinically and neuropathologically with multiple sclerosis (MS) according to the revised 2010 McDonald's criteria [76]. There, tissue samples were collected from MS patients, as approved by the Montreal-based CRCHUM research ethics committee. Autopsy samples were preserved and lesions classified using Luxol Fast Blue/Haematoxylin and Eosin staining and Oil Red-O staining, as previously published [14, 48]. No inflamed tissue areas were used in the current study. Additional, fresh-frozen and paraffin-embedded human samples were obtained from the Neuropathology Service at Brigham and Women's Hospital in Boston, MA

and from archived autopsy specimens in the Department of Pathology and Laboratory Medicine of The Ottawa Hospital, Ottawa, ON. Human spinal cord and muscle tissues were collected *post mortem* from organ donors at The Ottawa Hospital with approval from the Ottawa Health Science Network Research Ethics Board.

Animal tissues

All animal protocols were approved by the review board of the Animal Care and Veterinary Services at the University of Ottawa. Brains were collected from wild-type C57Bl/6J mice from Jackson laboratories (Bar Harbor, ME); *prkn*-null mice were from Dr. Brice's laboratory [34] and back-crossed onto a pure C57Bl/6J background; *Sod2*[±] mice were from Jackson laboratories (pure C57Bl/6J background), and the bi-genic mouse (*prkn*^{-/-}/*Sod2*[±]) was created by crossing *prkn*-null mice with *Sod2*-haploinsufficient mice, and the interbreeding of heterozygous offspring. These bi-genic mice have been characterized elsewhere (El-Kodsi et al. in preparation [17]). Following euthanasia by Euthanyl (65 mg/mL) intraperitoneal injection, mouse brains were collected and processed on ice in a Dounce glass homogenizer by 20 passes in Tris salt buffer with vs. without the addition of 1% hydrogen peroxide (H₂O₂—Sigma), or 0.1–1 M dithiothreitol (DTT—Sigma), transferred to ultracentrifuge tubes and spun during 30 min at 163,202.1 × *g* and 4 °C to extract the soluble fraction. The resulting pellets were further homogenized in the tris-salt buffer with the addition of 2–10% SDS, transferred to ultracentrifuge tubes and spun at 163,202.1 × *g* and 10 °C for 30 min to extract the insoluble fraction. Wild-type mice (of C57Bl/6J or mixed background, as indicated) were used for the analysis of the effects of PMI on murine parkin distribution in the brain. Mice ranging from 4 to 22 months in age were perfused with PBS, their brains collected and processed, as above. Wild-type SAS Sprague Dawley rats were obtained from Charles River Laboratories; frozen frontal lobe specimens of a cynomolgus monkey were provided by the New England Primate Research Center.

Sequential extraction of parkin from neural tissue

Approximately 1 cm³ of the human frontal cortex and mid-brain specimens (age range, 5–85 years) were weighed and placed in 3 × volume/weight of Tris-salt buffer (TS; 5 mM Tris, 140 mM NaCl, pH 7.5) containing complete EDTA-free protease inhibitor cocktail, and 10 mM iodoacetamide (IAA, Bio-Rad). The samples were homogenized on ice in a Dounce glass homogenizer by 50 passes, transferred to ultracentrifuge tubes and spun at 163,202.1 × *g* and 4 °C for 30 min. The TS supernatant was transferred to a fresh tube and the pellet was extracted further with the addition of 3 × volume/weight of Triton X-100 buffer (TX, TS + 2%

Triton X-100). The samples were mixed by vortexing, incubated on ice for 10 min and centrifuged again using the same setting. The TX supernatant was transferred to a fresh tube and the pellet was extracted further with the addition of 3 × volume/weight of SDS buffer (SDS, TS + 2% SDS). The samples were mixed by vortexing, incubated at room temperature for 10 min and centrifuged again at 163,202.1 × *g* and 12 °C for 30 min. The SDS supernatant was transferred to a fresh tube and the pellet was either stored at – 80 °C or extracted further with the addition of 3 × volume/weight of 6 × non-reducing Laemmli buffer (LB, 30% SDS, 60% glycerol, 375 mM Tris; pH 6.8;), mixed by vortex and incubated at room temperature for 10 min. Samples were centrifuged again at 163,202.1 × *g* and 12 °C for 30 min and the LB supernatant was transferred to a fresh tube. Extracted proteins from TS, TXS and SDS buffers including pellet (20–30 µg) and 10–20 µL of LB extracts were run on SDS-PAGE using reducing (100 mM DTT) and/or non-reducing (0 mM DTT) LB. Following transfer to membranes, Ponceaus S staining (Sigma) was used to probe for equal loading; following washing, membranes were immunoblotted for the detection of parkin (Biolegend 808503, 1: 5000), DJ-1 (Ab18257, 1: 2000), α-synuclein (syn-1, 1:1000 or MJFR-1, 1:2000), LC3B (3868, 1:2000), VDAC (MSA03, 1:5000), MnSOD and GLO1 (each at 1:1000), calnexin (MAB3126, 1:1000), cathepsin D (sc-6486, 1:1000), GRP75 (sc-1058, 1:1000). ImageJ software (version 1.52 k; National Institutes of Health, USA) was used for signal quantification purposes.

mRNA analyses

PRKN mRNA isolated from individual *S. nigra* dopamine neurons, cortical pyramidal neurons and non-neuronal, mononuclear cells from venous blood were processed, as described [16] and annotated in the Human BRAINcode database (www.humanbraincode.org).

1-methyl-4-phenyl-1,2,3,6-tetrahydropyridine (MPTP) treatment

Eight to 12 months-old wild-type and *prkn*-null mice were injected intraperitoneally with 40 mg/kg of saline or MPTP and sacrificed an hour later [3]. Brains were harvested for ROS measurement, protein analysis by Western blotting and immunoprecipitation of parkin followed by MS analysis. For LC–MS/MS, murine brains were first incubated in IAA prior to homogenization and fractionation, as described above. Brain homogenates were then incubated with anti-parkin conjugated to magnetic beads (Dynabeads Coupling Kit; Invitrogen), as below. A magnet was used to enrich mouse parkin bound to Prk8 conjugated to beads, and several washes were used to remove non-specific proteins. Eluted fractions (IP elute) along with controls (input, unbound,

wash and recombinant parkin protein standards) were run on SDS/PAGE under reducing conditions and blotted with anti-parkin. A sister gel was stained with Coomassie, as described above, and gel slices corresponding to band sizes at 50–75 kDa were excised and analyzed by LC–MS/MS, as described below.

Recombinant protein expression using a pET-SUMO vector

Plasmid cDNA encoding for wild-type and truncated (amino acid 321–465) human parkin proteins were expressed as 6His-Smt3 fusion proteins in *Escherichia coli* BL21 (DE3) Codon-Plus RIL-competent cells (C2527, New England Biolabs), as previously described [1, 49, 91]. Plasmids encoding for human parkin with p.C95A, p.G328E and p.C431F substitutions were generated with the use of a restriction-free cloning strategy [96] using the following primers: for p.C95A *PRKN* forward: CAGAAACGCGGCGGGAGG CgcTGAGCGGGAGCCCCAGAGCT and *PRKN* reverse: CATCCCAGCAAGATGGACCC; for p.G328E *PRKN* forward: TCCAAACCGGATGAGTGGTG and *PRKN* reverse: CGGGGGCATAACACGCCCcCATCTGCAGGACAC ACTC; for p.C431F *PRKN* forward: CTACTCCCTGCC TTGTGTGG and *PRKN* reverse: GCGGACACTTCATGT GCATaaGCCTCCATTTTTTCCACTGG.

DJ-1 and *SNCA* coding regions were cloned from pcDNA3.1 into the pET-SUMO vector using PCR and restriction enzymes. A new restriction site for NotI was inserted between SUMO cleavage site and protein start codon in pET-SUMO using the following primers: *pET-SUMO* forward: GTGATGCCGCCACGATGCGTCCG GC and *pET-SUMO* reverse: TTTTAAGCTTCCgcgccgc-CACCACCAATCTGTTC. The inserts containing wild-type *DJ-1* and *SNCA* sequences with 5' NotI and 3' HindIII restriction sites were generated using the following primers and inserted into pET-SUMO using standard conditions: for *DJ-1* forward: agggcgccgcATGGCTTCCAAA and *DJ-1* reverse: cctaagcttCTAGTCTTTAAGAACAAGTGGAGC CTTC; for *SNCA* forward: agggcgccgcATGGATGTATTC ATGAAAGG and *SNCA* reverse: ctTTAAGCTTCAGGTTT GTAGTCTTGATACCCTTCAGA.

Quality control steps were performed at the Sequencing Core Facility of the Ottawa Hospital Research Institute (OHRI) to confirm the correct sequences.

Transformed bacteria were grown at 37 °C in 2% Luria Broth containing 30 mg/L kanamycin. All parkin protein-expressing cultures were supplemented with 0.5 mM ZnCl₂. Protein expression was induced at 16 °C with isopropyl β-D-1-thiogalactopyranoside (Sigma) using 25 μM for wild-type parkin, and 0.75 mM for truncated parkin, DJ-1, α-synuclein and ulp1 protease. Bacteria were harvested after 16–20 h by centrifugation and resuspended

in isolation buffer, T500i (50 mM Tris, 500 mM NaCl, 250 μM TCEP, 25 mM imidazole, pH 7.5). Lysozyme (0.1 mg/mL, except for ulp1 protease) treatment and sonication steps (Sonic Vibra Cell) were used to lyse cells. Proteins were collected after 1 h incubation at 4 °C with Ni–NTA agarose and washed several times with buffers T500i and T200i (50 mM Tris, 200 mM NaCl, 250 μM TCEP, 25 mM imidazole, pH 7.5). Fractions of elution buffer T200e (50 mM Tris, 200 mM NaCl, 250 μM TCEP, 250 mM imidazole, pH 7.5) were combined with 2–2.5 mg of 6xHis-tagged ulp1 protease and subsequently dialyzed (6–8 kDa cut-off,) against T200 (50 mM Tris, 200 mM NaCl, 250 μM TCEP, pH 7.5) for 24 h at 4 °C. Remaining proteins were incubated with Ni–NTA agarose for 1 h at 4 °C. Fractions were collected until no protein was detectable, pooled and concentrated to 1 mg/mL using 10 kDa cut-off centrifugation filters (Millipore). The purity and correct masses of isolated proteins were assessed using electron spray ionization mass spectrometry (Agilent 6538 Q-TOF).

Protein staining methods

All proteins were separated on pre-cast 4–12% Bis–Tris SDS-PAGE gels (NPO321BOX, NPO322BOX, NPO336BOX) from Invitrogen using MES running buffer (50 mM MES, 50 mM Tris, 1 mM EDTA and 0.1% SDS, pH 7.3) and Laemmli loading buffer (10% SDS, 20% glycerol, 0.1% bromophenol blue, 0.125 M Tris HCl, 200 mM DTT or β-mercaptoethanol). Proteins were stained in gel using SilverQuest™ Silver Staining Kit (LC6070) from Invitrogen or Coomassie brilliant blue R-250 dye (20,278) from Thermo Scientific using the following protocol: The gel was transferred to a plastic container and rocked for 30 min in Fix Solution (10% acetic acid, 50% methanol), followed by staining for 2–24 h (0.25% Coomassie R250) until the gel turned a uniform blue. The stain was replaced with Destain Solution (7.5% acetic acid and 5% methanol) and the gel was rocked until crisp blue bands appeared. Following a wash with water, the gel was stored in 7% acetic acid. Proteins transferred to PVDF (Bio-Rad) membranes were stained with Ponceau S solution (Sigma) for 20 min, washed three times with water, imaged and then destained with 0.1 M NaOH prior to Western blotting.

Dynamic light scattering assay

For each recombinant protein preparation tested, the buffer (50 mM Tris, 200 mM NaCl and 250 μM TCEP, pH 7.5) was exchanged for a 20 mM phosphate buffer with 10 mM NaCl (pH 7.4). 20 μM full-length wild-type recombinant parkin was centrifuged at 21,000 × g for 60 min at 4 °C and

light scattering intensity of the supernatant was collected 30 times at an angle of 90° using a 10 s acquisition time. Measurements were taken at 37 °C using a Malvern Zetasizer Nano ZS instrument equipped with a thermostat cell. The correlation data were exported and analyzed using the nanoDTS software (Malvern Instruments). The samples were measured at 0, 1, 3 and 5 h. Following 24 h incubation, 2 mM DTT was added to the sample and the light scattering intensity of the supernatant was measured again.

Far UV circular dichroism spectroscopy

Fifteen μM of reduced and partially oxidized full-length wild-type, recombinant (r-) parkin was measured at $t=0$ and $t=5$ days of incubation under native conditions in 20 mM phosphate, 10 mM NaCl buffer. The aggregate-rich phase and the monomer-rich phase in the samples were separated with ultracentrifugation (100,000 × g for 2 h). Far UV circular dichroism (CD) spectra were recorded for the monomer- and aggregate-rich phase of protein samples using a JASCO J-720 spectrometer. The final spectrum was taken as a background-corrected average of 5 scans carried out under the following conditions: wavelength range 250–190 nm at 25 °C; bandwidth was 1 nm; acquisition time was 1 s and intervals was 0.2 nm. Measurements were performed in a 0.01 cm cell. CD spectra were plotted in mean residue ellipticity units (deg cm² dmol⁻¹) calculated by the following equation: $[\Theta] = \Theta_{\text{obs}} / (10ncl)$, where $[\Theta]$ is the mean residue molar ellipticity as a function of wavelength, Θ_{obs} is the measured ellipticity as a function of wavelength (nm), n is the number of residues in the protein, c is the concentration of the protein (M), and l is the optical path length (cm). Secondary structure analysis of proteins using CD spectroscopic data was carried out using the BeStSel (Beta Structure Selection) software [41, 61, 62, 90].

Cysteine labeling for mass spectrometry

Recombinant protein samples were first prepared by exchanging the T200 buffer for PBS. The protein concentrations were measured and adjusted to 10 μM using PBS. Stock solutions of 500 mM DTT, 100 mM IAA, 100 mM H₂O₂ and 250 mM EDTA were prepared in PBS. A stock of 500 mM NEM was prepared in ethanol immediately before use. The stepwise Cys labeling procedure was as follows: A 10 μL aliquot of protein (at 10 μM) was reacted with hydrogen peroxide at various concentrations, as indicated (Supplementary Table 2, online resource) for 30 min at 37 °C as indicated. Any unreacted cysteines were alkylated with incubation with 5 mM IAA (either with or, in some runs, without 10 mM EDTA) for 2 h at 37 °C. Previously oxidized cysteines were then reduced by treatment with 40 mM DTT for 30 min at 37 °C. Newly reduced cysteines were alkylated

by incubation with 85 mM *N*-ethyl maleimide (NEM) for 2 h at 37 °C. The samples were separated on SDS-PAGE using Laemmli buffer containing 100 mM DTT and proteins visualized using Coomassie staining. Appropriate bands were excised and analyzed by liquid chromatography mass spectrometry (LC–MS/MS).

Protein identification by LC–MS/MS

Proteomic analyses were performed at the OHRI Proteomics Core Facility (Ottawa, Canada). Proteins were digested in-gel using trypsin (Promega) according to the method of Shevchenko [84]. Peptide extracts were concentrated by Vacufuge (Eppendorf). LC–MS/MS was performed using a Dionex Ultimate 3000 RLSC nano HPLC (Thermo Scientific) and Orbitrap Fusion Lumos mass spectrometer (Thermo Scientific). MASCOT software version 2.6.2 (Matrix Science, UK) was used to infer peptide and protein identities from the mass spectra. For detection of dopamine metabolites on parkin, the following variable modifications were included: 5,6-indolequinone (+ C₈O₂NH₃, m/z shift + 145), aminochrome (+ C₈O₂NH₅, + 147), aminochrome + 2H (+ C₈O₂NH₇, + 149), and dopamine quinone (+ C₈O₂NH₉, + 151). These samples were prepared for analysis without any use of DTT or IAA. The observed spectra were matched against human sequences from SwissProt (version 2018-05) and also against an in-house database of common contaminants. The results were exported to Scaffold (Proteome Software, USA) for further validation and viewing.

Analysis of the r-parkin holoprotein and of three runs of H₂O₂-exposed r-parkin (Supplementary Table 2, online resource) was also performed at the University of Western Ontario. There, samples were run on a QToF Ultima mass spectrometer (Waters) equipped with a Z-spray source and run in positive ion mode with an Agilent 1100 HPLC used for LC gradient delivery (University of Western Proteomics Facility).

MaxQuant analysis of mass spectrometry data

For select experiments, the raw MS data files were further processed with MaxQuant software version 1.6.5 and searched with the Andromeda search engine [10]. The reference fastas were set to uniprot-human (version 2019-02-12) and uniprot-ecoli. The *E. coli* proteome was included to account for bacterial proteins present in the recombinant protein samples. The ‘second peptides’ and ‘match between runs’ settings were enabled. All other settings were left as default. Selected variable modifications included oxidation (Met), acetylation (protein N-terminus), and carbamidomethyl (Cys), as well as custom modifications for pyro-carbamidomethyl (N-terminal Cys), N-ethylmaleimide (Cys), and

NEM + water (Cys). For data analyses, site-level intensity values were obtained from the MaxQuant-generated “CarbamidomethylSites” table which combines the intensity of MS1 signals from all peptides covering a particular cysteine residue.

Immunoprecipitation (IP) of brain parkin

Conjugation of anti-parkin antibody (Prk8, 808503, lot B209868) and clone A15165-B (this report: Suppl. Figure 8c) to magnetic beads at a final concentration of 10 mg of antibody/mL of beads was carried out following the Magnetic Dynabeads Antibody Coupling Kit from Invitrogen (14311D). Human tissue lysates were also prepared using the sequential extraction of proteins from neural tissue protocol, as described above, with the addition of 10 mM IAA prior to homogenization. Equal amounts of protein from TS tissue extracts ($n=4$) and SDS tissue extracts ($n=8$) were diluted in TS buffer, resulting in final SDS concentrations of 0.0175–0.05% in the SDS extracts. For the IP, anti-parkin primary antibody-conjugated agarose beads were first prepared by multiple washes with 1 mL of TS buffer using centrifugation ($1000\times g$ at $4\text{ }^{\circ}\text{C}$ for 3 min) and adhesion to a strong magnet. The amount of Prk8 conjugated agarose beads used for each experiment were approximated based on the amount of parkin (μg)/sample calculated by densitometry when the sample was compared to recombinant parkin protein standards using Western blotting with Prk8 as a primary antibody. The mixture was incubated for 16 h at $4\text{ }^{\circ}\text{C}$ with slow rotation. Unbound proteins, were separated from the beads by centrifugation ($1000\times g$ at $4\text{ }^{\circ}\text{C}$ for 3 min) followed by adhesion to a strong magnet and saved as the IP “unbound” fraction.

Beads were washed three times with 1 mL of ice-cold RIPA buffer (1% nonionic polyoxyethylene-40, 0.1% SDS, 50 mM Tris, 150 mM NaCl, 0.5% sodium deoxycholate, 1 mM EDTA) using centrifugation ($1000\times g$ at $4\text{ }^{\circ}\text{C}$ for 3 min) and adhesion to a strong magnet. Approximately 5–10 μL of each wash was combined and saved as the IP “wash” fraction. To elute antibody-bound proteins, 35 μL of 6X reducing Laemmli buffer (30% SDS, 60% glycerol, 0.3% bromophenol blue, 0.375 M Tris, 100 mM DTT, pH 6.8) was added to the beads and the samples were boiled for 5 min. Following centrifugation ($1000\times g$ at $4\text{ }^{\circ}\text{C}$ for 3 min), the supernatant was transferred to a fresh tube labeled “IP elute” and the beads were discarded. To assess IP efficiency, eluted fractions (IP elute), along with controls (input, unbound, wash and recombinant parkin protein standards) were run on SDS/PAGE and blotted with anti-parkin antibody (Prk8, MAB5512 Millipore or 2132S Cell Signalling). Human IP elutes used for mass spectrometry (MS) analysis were incubated with 500 mM NEM (as indicated for select runs) for 16 h at $4\text{ }^{\circ}\text{C}$ prior to SDS-PAGE and further processed for MS, as described above. Gel slices

corresponding to band sizes at 50–53 kDa were excised and analyzed by LC–MS/MS.

Reactive oxygen species (H_2O_2) measurements in recombinant protein preparations, cell lysates and tissue homogenates

An Amplex[®] Red hydrogen peroxide/peroxidase assay kit (Invitrogen A22188) was used to monitor endogenous levels of H_2O_2 in aliquots of tissues and cells, and in test tubes following either exposure to increasing concentrations of H_2O_2 , *n*-ethylmaleimide (NEM), and ethylenediaminetetraacetic acid (EDTA), or after incubation with either select, recombinant parkin proteins, or DJ-1, α -synuclein, bovine serum albumin (Thermo Scientific), ring finger protein 43 (RNF43—BioLegend, MA.), HOIL-1-interacting protein (HOIP—Boston Biochem, MA.), glutathione (Sigma), or catalase (Sigma) for 30 min at room temperature. Pre-weighed cortex pieces from the human brain and pelleted cells were homogenized on ice in the $1\times$ reaction buffer provided (Invitrogen A22188) using a Dounce homogenizer ($3\times$ volume to weight ratio). Homogenates were diluted in the same $1\times$ reaction buffer (fivefold to tenfold). A serial dilution of the H_2O_2 standard provided was prepared (20, 10, 2 and 0 μM). Fifty μL of standards and samples were plated in a 96-well black plate with a clear flat bottom (Thermo Fisher Scientific). The reaction was started by the addition of 50 μL reaction buffer, Amplex[®] Red and horseradish peroxidase (HRP) (10 mM Amplex[®] Red and 10 U/mL HRP). Plates were incubated at room temperature for 30 min protected from light. A microplate reader was used to measure either fluorescence with excitation at 560 nm and emission at 590 nm, or absorbance at 560 nm. The obtained H_2O_2 levels (μM) were normalized to the tissue weight (g) or protein concentration ($\mu\text{g}/\mu\text{L}$). The same assay was also used to measure parkin and glutathione’s peroxidase activity compared to horseradish peroxidase.

Chemiluminescence-based, direct reactive oxygen species assay

The assay was modified from Muller et al. [64] to measure the ROS-quenching ability of parkin proteins, DJ-1, GSH, and catalase. Protein concentrations were quantified using Bradford assay and adjusted to 5, 10, 15 and 30 μM in buffer not containing TCEP. Bovine serum albumin (BSA; 10 and 20 μM ; Thermo Scientific), glutathione (15, 20, 200, 400, 800 and 2000 μM ; Sigma), and catalase (15 μM , Sigma) were prepared. Stock solutions of H_2O_2 for standard curve were prepared at 5, 10, 20, 40 and 50 mM in 0.1 M Tris HCl pH 8.0 using 30% H_2O_2 . Stock solutions of 300 mM luminol and 40 mM 4-iodophenol were prepared in DMSO and protected from light. Signal reagent, containing 1.94 mM

luminol (Sigma) and 0.026 mM 4-iodophenol (Sigma), was prepared in 0.1 M Tris HCl pH 8.0 and protected from light. A 0.4% horseradish peroxidase solution was prepared using HRP-linked anti-rabbit secondary antibody diluted in Stabilizyme solution (SurModics SZ02). Each read was set up in triplicate on a white polystyrene 96-well plate (Thermo Scientific 236,105) and to each well was added 80 μ L Stabilizyme, 15 μ L of 0.4% horseradish peroxidase (HRP) and 25 μ L of sample or controls. One of the injectors in a Synergy H1Multi-Mode Plate Reader (Bio Tek) was primed and set to inject 15 μ L of signal reagent and 15 μ L of each H₂O₂ stock solution was manually added to corresponding controls and samples just prior to reading. Final concentrations of reagents were 0.04% HRP, 500, 1000, 2000, 4000 and 5000 μ M H₂O₂, 194 μ M luminol, 2.6 μ M 4-iodophenol and 0.8, 1.7, 2.5 or 5 μ M of protein. The plate reader was set to measure luminescence every 1 min for a total of 10 min.

The resulting kinetic data were converted to the area under the curve (AUC) using Prism software version 6. For samples pre-incubated with 20 mM iodoacetamide, a stock solution of 1 M iodoacetamide was prepared. To each well containing 25 μ L of the sample, 0.52 μ L of 1 M iodoacetamide and 0.48 μ L of buffer not containing TCEP was added and the samples were incubated for 2 h at 37 °C. Following incubation, the reagents for chemiluminescence were added as above except 79 μ L of Stabilizyme was used instead of 80 μ L and the samples were analyzed as above.

Thiol quantification in recombinant proteins

Recombinant protein samples were first prepared by exchanging the T200e protein buffer (50 mM Tris, 200 mM NaCl and 250 μ M TCEP, pH 7.5) for T200 using repeat centrifugations (8 times 4000 \times g at 4 °C for 10 min) in Amicon Ultra 10 kDa MWCO filters (Millipore). The protein concentrations were measured and recorded. A glutathione stock solution of 32,539 μ M was prepared by dissolving 1 mg glutathione (GSH) in 1 mL of T200 and the standards 0, 50, 101, 203, 406, 813 and 1000 μ M were prepared by serial dilution in T200. The reaction buffer (0.1 M sodium phosphate, pH 8.0) was prepared by adding 93.2 mL 1 M Na₂HPO₄ and 6.8 mL of NaH₂PO₄ in 1 L of water. Thiol detecting reagent (Ellman's reagent) was prepared by dissolving 2 mg of 5,5'-dithio-bis-[2-nitrobenzoic acid] (DNTB; Sigma) in 1 mL of reaction buffer. The assay was performed in 96-well clear round-bottom plates (Corning) by adding 50 μ L of thiol detecting reagent to 50 μ L of sample or standard and incubating for 15 min at room temperature.

The resulting 5-thio-2-nitrobenzoic-acid (TNB) produced was measured by absorbance at 412 nm using a Synergy H1Multi-Mode Plate Reader (Bio Tek). The amount of free thiols detected in each sample was calculated using the

regression curve obtained from the glutathione standards and dividing by the concentration of the sample.

Zinc ion release assay

A zinc quantification kit (Abcam—ab102507) was used to assay zinc ion (Zn²⁺) release from proteins. Recombinant human proteins (wild-type r-parkin and r-DJ-1) were spun in 10 or 30 kDa cut-off centrifugation filters (Millipore) to remove residual TCEP. Increasing concentrations of protein (0 to 2.5 μ M) were incubated under basal conditions or with the addition of H₂O₂ (2 mM) or DTT (100 mM) for 30 min at 37 °C. A standard curve was prepared using a zinc standard (stock, 50 mM) provided by the manufacturer. Two hundred μ L of the reaction mixture was added to 50 μ L standards and samples on 96 well plates (Thermo Fisher Scientific) followed by incubation at room temperature for 10 min. A microplate reader was used to measure the absorbance at OD560 nm. The background was corrected by subtracting the value derived from wells of zero zinc standard from all readings.

Cell cytotoxicity assay

Human neuroblastoma cell lines (M17) without transduction (controls), or transduced by vector-only plasmid (Myc-tag), or those with low levels of stable expression of Myc-parkin cDNA (P5) and high levels of stable expression of Myc-parkin (P17), or sister lines transiently over-expressing flag-parkin (wild-type), flag-vector and flag-parkin carrying one of three-point mutations (p.C431F; p.G3289E; p.C95A) were grown in 6-well culture plates at 0.3 \times 10⁶ cell density (80% confluence). There, Opti-MEM media (Gibco 11,052-021) contained heat-inactivated fetal bovine serum (Gibco 10,082-147), Pen/strep/Neo (5 mg/5 mg/10 mg; Gibco 15,640-055), MEM-non-essential amino acids (10 mM; Gibco 11,140-050) and sodium pyruvate (100 mM). For rescue experiments, M17 cells transiently expressing cDNA for flag-vector, flag-parkin wild-type, and variants carrying p.G328E, p.C431F, or p.C95A-encoding parkin protein were used. There, 4 μ g of cDNA was transfected using a 1:1 ratio of cDNA to Lipofectamine 2000 (52,887, Invitrogen) in OPTI-MEM transfection medium. Lipofectamine 2000 and cDNA were first incubated for 20 min at room temperature before being applied directly to the cells for 1 h at 37 °C with 5% CO₂ followed by direct addition of fresh growth medium. The cells were incubated another 20–24 h at 37 °C with 5% CO₂.

Dopamine hydrochloride (Sigma) 200 mM stock was prepared. Cells were washed with fresh media once and then incubated with media alone or supplemented with dopamine at final concentrations of 20 μ M and 200 μ M

for 18–20 h. Post dopamine exposure, conditioned media were collected for cytotoxicity assays and cells were harvested for lysis in TS buffer, vortexed and centrifuged. Supernatants were collected and saved for Western blot analyses and to be assessed for cytotoxicity. Cell pellets were suspended in 2–10% SDS buffer and centrifuged to collect the ‘insoluble fraction’.

Vybrant™ cytotoxicity assay kit (Molecular Probes V-23111) was used to monitor cell death through the release of the cytosolic enzyme glucose 6-phosphate dehydrogenase (G6PD) by damaged cells into the surrounding medium. Fifty µl of fresh media (without any exposure to cells) as well as conditioned media from control and stressed cells, in addition to lysates of M17 cells (as a positive control for maximum G6PD), were added to a 96-well microplate. Fifty µl of reaction mixture containing buffer (as per manufacturer) and resazurin, which reacts with G6PD generating fluorescently detectable resorufin, were added to each well, and the microplate was incubated at 37 °C for 30 min. A microplate reader was used to measure either fluorescence with excitation at 560 nm and emission at 590 nm, where the rise in fluorescence indicates a rise in G6PD levels as a surrogate marker of cell death.

Aminochrome synthesis

A solution of 0.1 M sodium phosphate buffer pH 6.0 was prepared from a mixture of 12 mL of 1 M NaH₂PO₄ and 88.0 mL of 1 M Na₂HPO₄. The reaction buffer (0.067 M sodium phosphate, pH 6.0) was prepared by adding 33 mL of 0.1 M sodium phosphate buffer to 17 mL water. A solution of 10 mM dopamine in reaction buffer was prepared by adding 19 mg of dopamine hydrochloride (Sigma) to 1 mL of reaction buffer. Oxidation was activated by adding 5 µL of tyrosinase (25,000 U/mL; Sigma) and the mixture was incubated at room temperature for 5 min. Tyrosinase was separated from the oxidized dopamine using a 50 kDa cut-off Amicon Ultra centrifugation filter (Millipore) by centrifuging at 21,000×g for 10 min. The absorbance of the filtrate was measured at a wavelength of 475 nm (Ultrospec 2100 pro spectrophotometer, Biochrom) and the concentration of aminochrome was determined using the Beer-Lambert equation and extinction coefficient of 3058 L × mol⁻¹ × cm⁻¹.

Redox chemistry reactions including oxidation of cysteine-containing proteins in vitro

Purified, recombinant proteins were prepared by removing excess TCEP, present in the elution buffer, by using repeat centrifugations (8 times 4000×g at 4 °C for 10 min) in Amicon Ultra 10 kDa MWCO filters (Millipore). Protein concentrations were measured and adjusted to 20 µM. Stock

solutions of hydrogen peroxide (H₂O₂, 9.8 mM) and aminochrome (as described above) and used at concentrations of 0–200 µM, were prepared. An aliquot of 10 µL of each protein sample (at 20 µM) was reacted with oxidants at the following concentrations: 0, 20, 200, 500, 750, 1000, 2000 µM for H₂O₂, and 0, 10 µM, 100 µM, 1 mM, 10 mM, 100 mM, 1000 mM for DTT. Samples were treated for 30 min at 37 °C and centrifuged at 21,000×g for 15 min. The supernatant was transferred to a fresh tube and the remaining pellet was extracted with 10 µL of T200 containing either 10% SDS or 100 mM DTT. The pellets were incubated again for 30 min at 37 °C and centrifuged at 21,000×g for 15 min. Laemmli buffer (10 µL, containing 100 mM mercaptoethanol) was added to both the pellet and supernatant fractions and samples were separated by SDS-PAGE and visualized by silver staining. Specific bands of aminochrome-treated wild-type, full-length r-parkin were excised and analyzed by LC-MS/MS, as described above.

In vitro melanin formation assay

Recombinant protein samples were first prepared by exchanging the T200e protein buffer (50 mM Tris, 200 mM NaCl and 250 µM TCEP, pH 7.5) for T200 (50 mM Tris and 200 mM NaCl, pH 7.5) using repeat centrifugations (8 times 4000×g at 4 °C for 10 min) in Amicon Ultra 10 kDa MWCO filters (Millipore). The protein concentrations were measured and adjusted to 20 µM using T200. A 0.067 M sodium phosphate buffer, pH 6.0, was prepared by adding 33 mL of 0.1 M sodium phosphate buffer to 17 mL water and adjusting the pH using HCl. A stock solution of 100 mM dopamine hydrochloride was prepared in 0.067 M sodium phosphate buffer and stock solutions of 100 mM reduced glutathione and H₂O₂ were prepared in T200.

Samples and controls were prepared in 100 µL total volume that contained 10 µL of protein sample or T200, 10 µL of 100 mM dopamine or 0.067 M sodium phosphate buffer, 10 µL of 100 mM glutathione or T200 buffer, and 70 µL T200. Unless otherwise indicated, the final concentration of protein was 2 µM and the final concentration of reagents was 10 mM. The samples and controls were plated in triplicate, and absorbance read at 405 and 475 nm every 90 s for 1 h and up to 4 h (Synergy H1Multi-Mode Plate Reader; Bio Tek).

Immunohistochemistry

Immunohistochemistry (IHC) was performed on paraffin-embedded sections, as previously described [81, 82, 87]. Briefly, prior to antibody incubation, sections were deparaffinized in xylene and successively rehydrated through a series of decreasing ethanol concentration solutions. Endogenous

peroxidase activity was quenched with 3% hydrogen peroxide in methanol, followed by a standard citric acid-based antigen retrieval protocol (CitriSolv, Decon Labs) to unmask epitopes. Sections were blocked in 10–20% goat serum in PBS-Tween (Tween 20 0.075%) to reduce non-specific signal. Sections were incubated overnight at 4 °C in primary antibodies diluted in 1–5% goat serum in PBS-T according to the following concentrations: novel anti-parkin mAbs from Biolegend clones D (BioLegend, A15165-D; 1:250), clone E (BioLegend, A15165E; 1:2,000), and clone G (1:250), Prk8 (BioLegend, MAB5512; 1:500) as well as anti-LAMP-3/CD63 (Santa Cruz, SC5275; 1:100), anti-LC3B (Sigma, L7543-200uL; 1:100), anti-VDAC (MitoScience, MSA03; 1:100). Biotinylated, secondary antibodies (anti-mouse IgG (H+L), Vector Labs, BA-9200, and biotinylated anti-rabbit IgG (H+L), both made in goat; Vector Labs, BA-1,000) were diluted to 1:225, and sections were incubated for 2 h at room temperature. The signal was amplified with VECTASTAIN® Elite® ABC HRP Kit (Vector Labs, PK-6100), and visualized via standard diaminobenzidine solution (DAB, 55 mM), or Vina green (Biocare Medical, BRR807AH), or most frequently by using ‘metal enhanced DAB’ (Sigma, SIGMAFAST™ DAB with Metal Enhancer D0426). Samples were counterstained with Harris Modified Hematoxylin stain and dehydrated through a series of increasing ethanol concentration solutions and xylene. Permount (Fisher Scientific, SP15-100) was used for mounting and slides processed for IHC were visualized and processed using a Quorum Slide Scanner at the OHRI Imaging Core Facility.

Immunofluorescence and confocal microscopy

Paraffin-embedded human midbrain sections were stained by routine indirect immunofluorescence (IIF) with the following details. Antigen retrieval was performed in Tris–EDTA buffer pH 9.0 for 10 min. Primary antibodies were incubated overnight at 4 °C. Details for primary antibodies anti-parkin clone E (1:500), anti-LAMP-3 (1:250) are described above. Fourty min-long incubations with the following secondary antibodies were performed: goat anti-mouse alexa fluor 488 (1:200), goat anti-rabbit alexa fluor 594 (1:500). Slides were mounted with fluorescence mounting medium using DAPI. Sections stained for IIF were imaged using a Zeiss LSM 880 AxioObserver Z1 with an Airyscan Confocal Microscope and then processed for further analysis using Zeiss Zen and Fiji software.

Statistical analyses

Statistical analyses were performed using GraphPad Prism version 6 (GraphPad Software, San Diego, CA, USA, www.graphpad.com).

Differences between two groups were assessed using an unpaired *t*-test. Differences among 3 or more groups were assessed using a one-way or two-way ANOVA followed by Tukey’s post hoc corrections to identify statistical significance. Select post hoc tests are depicted graphically to visualize significance. For all statistical analyses, a cut-off for significance was set at 0.05. Data are displayed with *p* values represented as **p* < 0.05, ***p* < 0.01, ****p* < 0.001, and *****p* < 0.0001. Linear regression (for the continuous dependent variable, e.g., % soluble parkin and H₂O₂ concentration) was performed using R version 3.6.0. Furthermore, to address the effect of age on parkin solubility (defined as a dichotomous variable using criteria below), logistic regression and receiver operating characteristic (ROC) curves and area under the ROC curve (AUC) values were calculated using R, as reported [87].

Results

Parkin solubility declines in the ageing human brain including in the *Substantia nigra*

Parkin’s biochemistry in the human brainstem vs. other regions of the neuroaxis has remained largely unexplored [73]. We serially fractionated 20 midbrain specimens (ages, 26–82 years) and > 40 cortices (ages, 5–85 years) from human subjects, which had been collected *post mortem* (Fig. 1, Supplementary Fig. 1; Supplementary Table 1, online resource). In control brain, we found that before the age of 20 years, nearly 50% of cortical parkin was found in soluble fractions generated by salt [Tris-NaCl; TS]- and non-ionic detergent [Triton X-100; TX]-containing buffers (Fig. 1a, b; Supplementary Fig. 1a, online resource). In contrast, after age 50 years, parkin was predominantly (> 90%) found in the 2% SDS-soluble (SDS) fraction and the 30% SDS extract of the final fractionation pellet (P). The same distribution was seen in adult midbrain (e.g., *S. nigra*; red nucleus), the pons (e.g., *L. coeruleus*), and the striatum (Fig. 1a, b; Supplementary Fig. 1a–c, online resource).

Intriguingly, in older individuals (ages, ≥ 50 years) approximately half of the detectable parkin remained soluble in the human spinal cord and skeletal muscle specimens, which had also been collected *post mortem* (Fig. 1c, d). We used univariate linear regression analysis to explore a correlation between soluble parkin (of TS- and TX-fractions relative to the total signal for parkin, plotted as %) and age in human control cortices (Fig. 1e). The regression coefficient of age was – 0.54 (at a 95% confidence interval (CI) of – 0.79 to – 0.29, *P* = 7.7e^{–05}), where the multiple R-squared value was 0.302. When defining parkin solubility as a binary variable, i.e., the presence or absence of soluble parkin in TS- and TX-fractions (absent defined as less than 2% of total

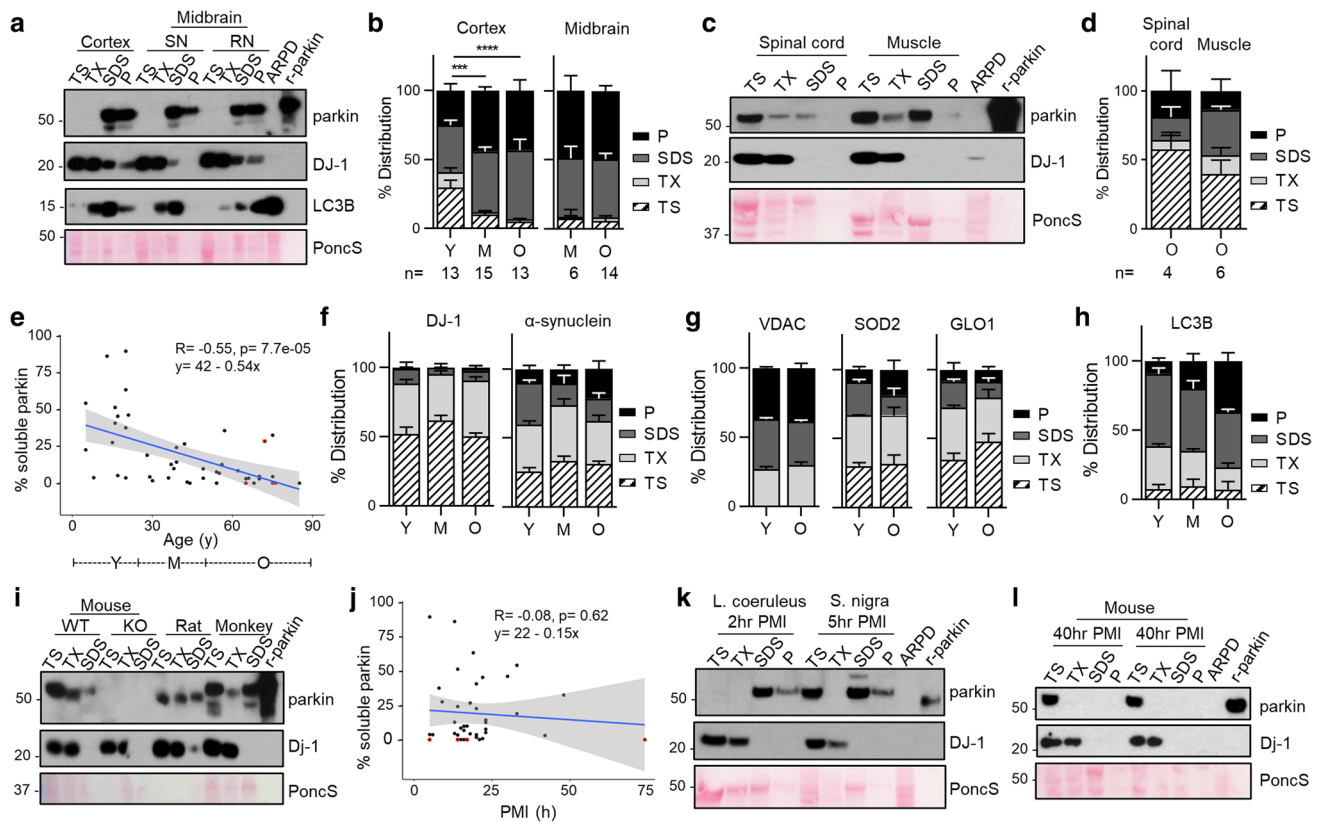


Fig. 1 Parkin's decline in solubility is specific to the adult human brain and correlates with age. **a** Representative Western blots of parkin, DJ-1, and LC3B distribution in human cortex, *S. nigra* (SN) and red nucleus (RN) serially fractionated into Tris-NaCl buffer-soluble (TS), Triton X-100-soluble (TX), 2% SDS-soluble (SDS) extracts and the pellet (P) lysed in 30% SDS-containing buffer. SDS extracts from *PRKN*-linked Parkinson disease (ARPD) brain and recombinant, human parkin (r-parkin) are included. Ponceau S is shown as loading control. **b** Relative distribution of parkin signal within each fraction for cortex and midbrain grouped by age ranges: young (Y ≤ 20 years; $n = 13$); mid (M > 20 years but < 50 years; $n = 15$ for cortex, and $n = 6$ for midbrain); older (O ≥ 50 years; $n = 13$ for cortex and $n = 14$ for midbrain). Data shown as mean \pm SEM. The significance in protein distribution between soluble (TS+TX) and insoluble (SDS+pellet) fractions was determined using 2-way ANOVA [$F(2, 76) = 26.21$, $p < 0.001$] with Tukey's post hoc test ($***p < 0.001$; $****p < 0.0001$). Additional Western blots are shown in Supplementary Fig. 1a–c, online resource. Midbrains include both control and neurological disease cases, as listed in Supplementary Table 1, online resource. **c** Western blots of parkin and DJ-1 as well as Ponceau S staining of serial fractions from the representative human spinal cord and skeletal muscle tissues from individuals ≥ 50 years. **d** Relative distribution of parkin as in (b) for human spinal cord ($n = 4$) and skeletal muscle specimens ($n = 6$) from donors aged 50–71 years. **e** Univariate linear regression analysis of parkin solubility in cortices as a function of age ($n = 46$). Each brain is represented by an individual dot; red circles denote three cases of parkinsonism not linked to *PRKN*; the linear regression line (in blue) and 95% confidence intervals (grey) are shown. Age ranges that correspond to Y–O–M in (b) are shown under the graph. Age coefficient was -0.54 (95% CI: -0.79 to -0.29 , $P = 7.7e^{-05}$). **f–h** Relative distribution of **f** DJ-1, α -synuclein and **g** VDAC, MnSOD, glyoxalase (GLO1) and **h** LC3B in human cortices ($n = 3–5$ per age group), as described in (b). Representative Western blots are shown in Supplementary Fig. 1b, c, online resource. **i** Western blots of parkin and DJ-1 and Ponceau S staining of serial fractions from whole brains of wild-type (WT; 8 months of age) and *prkn* knock-out (KO) mice, WT rat (WT; 14 months) and from frontal cortex of a cynomolgus monkey (60 months). **j** Univariate linear regression analysis of parkin solubility in human brain as a function of length for *post mortem* interval (PMI; in hours); the linear regression line (in blue) and 95% confidence intervals (grey) are shown ($n = 41$ cortices). **k** Western blots of parkin and DJ-1 distribution in two human brainstem nuclei, *L. coeruleus* and *S. nigra*, which were collected within 2–5 h after death prior to freezing and processed as in (a, c). **l** Immunoblots for endogenous parkin and DJ-1 as well as Ponceau S staining from serially extracted WT mouse brains ($n = 3$) dissected after a 40 h *post mortem* interval. Note, Western blots shown in this figure followed SDS/PAGE under reducing conditions

signal), and using logistic regression analysis, we found that the transition to insoluble parkin occurred between the ages of 28 years (with low sensitivity but high specificity values) and 42 years (with high sensitivity and low specificity values) (data not shown).

regression analysis of parkin solubility in cortices as a function of age ($n = 46$). Each brain is represented by an individual dot; red circles denote three cases of parkinsonism not linked to *PRKN*; the linear regression line (in blue) and 95% confidence intervals (grey) are shown. Age ranges that correspond to Y–O–M in (b) are shown under the graph. Age coefficient was -0.54 (95% CI: -0.79 to -0.29 , $P = 7.7e^{-05}$). **f–h** Relative distribution of **f** DJ-1, α -synuclein and **g** VDAC, MnSOD, glyoxalase (GLO1) and **h** LC3B in human cortices ($n = 3–5$ per age group), as described in (b). Representative Western blots are shown in Supplementary Fig. 1b, c, online resource. **i** Western blots of parkin and DJ-1 and Ponceau S staining of serial fractions from whole brains of wild-type (WT; 8 months of age) and *prkn* knock-out (KO) mice, WT rat (WT; 14 months) and from frontal cortex of a cynomolgus monkey (60 months). **j** Univariate linear regression analysis of parkin solubility in human brain as a function of length for *post mortem* interval (PMI; in hours); the linear regression line (in blue) and 95% confidence intervals (grey) are shown ($n = 41$ cortices). **k** Western blots of parkin and DJ-1 distribution in two human brainstem nuclei, *L. coeruleus* and *S. nigra*, which were collected within 2–5 h after death prior to freezing and processed as in (a, c). **l** Immunoblots for endogenous parkin and DJ-1 as well as Ponceau S staining from serially extracted WT mouse brains ($n = 3$) dissected after a 40 h *post mortem* interval. Note, Western blots shown in this figure followed SDS/PAGE under reducing conditions

This age-dependent partitioning of parkin was not seen for any other protein examined, including two other PD-linked proteins, i.e., DJ-1 and α -synuclein (Fig. 1a, f), or for organelle-associated markers, e.g., cytosolic glyoxalase-1, peroxiredoxin-1 and -3; and endoplasmic reticulum-associated calnexin. Notably, mitochondrial

markers, e.g., voltage-dependent anion channel (VDAC) and Mn²⁺-superoxide dismutase (MnSOD), also did not partition with parkin (Fig. 1g; Supplementary Fig. 1b, c, online resource; and data not shown). In contrast, parkin did co-distribute with LC3B, a marker of protein aggregation, foremost in brain specimens from older individuals (Fig. 1a, h; Supplementary Fig. 1c, online resource).

The age-associated loss in parkin solubility appeared unique to the human brain in that it remained predominantly soluble in the adult nervous system of other species, e.g., mice and rats as well as cynomolgus monkey, which were processed in the same way (Fig. 1i). Specifically, in brain lysates of two different wild-type strains of mice (C57Bl/6J, and a mixed 129S1/FVB/N//C57Bl/6J background) aged to 18 and 22 months respectively, parkin remained present in the soluble fraction throughout their lifespan (Supplementary Fig. 1d, online resource; and data not shown).

In soluble fractions from older humans, we did not detect any truncated species of parkin using several, specific antibodies (data not shown). Despite the loss of parkin solubility with progression in age, *PRKN* mRNA was detectable in individual neurons isolated from the *S. nigra* and cortex throughout all age groups; there, transcript levels in neurons did not correlate with the subject's age (Supplementary Fig. 1e, f, online resource).

Our analysis comprised samples with *post mortem* intervals (PMI) that spanned from 2 to 74 h (Supplementary Table 1, online resource). Using univariate linear regression analysis, we detected no correlation between parkin solubility in human control cortices ($n=41$) and PMI length, where the regression coefficient for PMI measured -0.15 (95% CI: -0.76 to 0.46 , $P=0.62$), and the multiple R-squared value was 0.0064 (Fig. 1j). As expected, PMI did not correlate with the age of the deceased person (not shown). Likewise, wild-type parkin was found to be largely insoluble in striatal, midbrain and pontine samples isolated from aged subjects with PMIs as short as 2 to 6 h (Fig. 1k; Supplementary Fig. 2a, b, online resource). We further explored a possible contribution of PMI to parkin solubility by mimicking conditions of some of the human autopsy cases, using adult mice. This included a PMI length of up to 40 h, where animals were kept at room temperature for the first 14 h, followed by storage over 26 h at 4 °C before removal of their brain; in these cases, parkin remained in the soluble compartments (Fig. 1l and data not shown). While we cannot exclude that PMI length could affect parkin's solubility in some cases, the age-dependent loss of parkin solubility observed in human brain samples of our cohort was not due to the PMI.

Further, we determined that the decline in detectable parkin solubility in the aged human brain did not differ based on the sex of the deceased person, such as when examined by univariate linear regression analysis or by multivariate

analysis (data not shown); it was also not caused by either tissue freezing prior to protein extraction or the pH value of the buffer (Supplementary Fig. 2c–f, online resource). Moreover, employing the commonly used 'RIPA buffer' instead of our serial extraction buffers resulted in the release of parkin into the supernatant with some reactivity left in the pellet, as expected (Supplementary Fig. 2g, online resource).

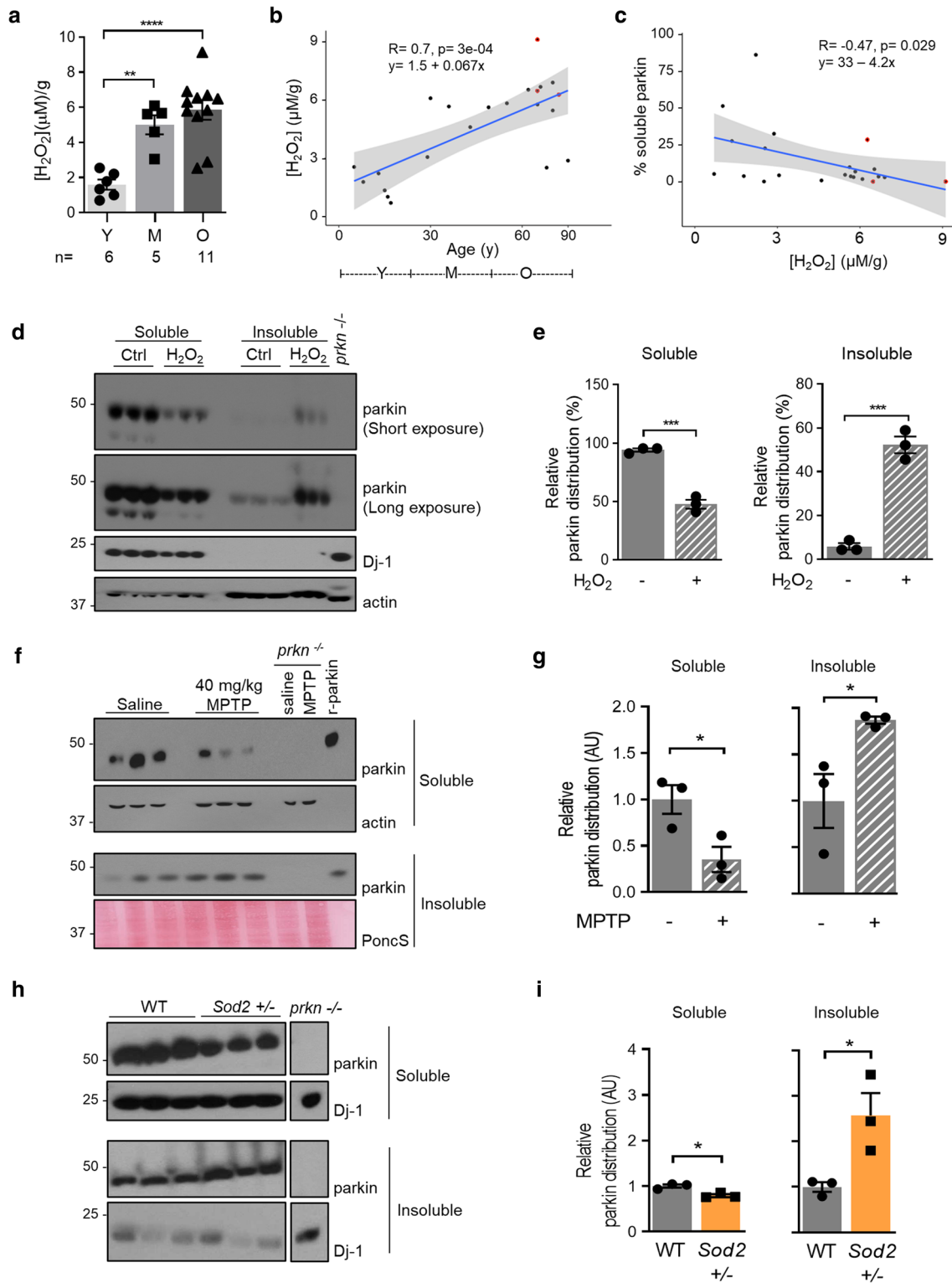
Decline in parkin solubility correlates with rising hydrogen peroxide levels in the mammalian brain

We next explored a possible association between parkin distribution, age and oxidative changes. Using sister aliquots from the brain specimens examined above, we found that hydrogen peroxide (H₂O₂) concentrations positively correlated with age (Fig. 2a, b; see also Supplementary Table 1, online resource), as expected from the literature [54]. Using univariate linear regression analysis, we determined that the coefficient of age was 0.067 (95% CI: 0.035 to 0.098 , $P=3e^{-04}$; multiple R-squared value, 0.4877).

In three brains from subjects with non-*PRKN*-linked parkinsonism, the levels of H₂O₂ were similar to those measured in age-matched controls (Fig. 2b). When analyzing parkin distribution vs. H₂O₂ concentrations in human cortices, we found that parkin solubility in human brain negatively correlated with H₂O₂, where the coefficient of the latter was -4.2 (95% CI: -7.92 to -0.48 , $P=0.029$; multiple R-squared value, 0.2174) (Fig. 2c).

We next sought to dynamically model the observed correlation between higher ROS levels in the nervous system and reduced parkin solubility. We first used an *ex vivo* approach, whereby wild-type mouse brains were exposed to either saline or H₂O₂ during tissue homogenization. There, we saw a significant reduction in soluble parkin and an increase in insoluble parkin in the H₂O₂-exposed lysates (Fig. 2d, e). We next examined two *in vivo* models. In the first, wild-type mice were intraperitoneally injected with 40 mg/kg of 1-methyl-4-phenyl-1,2,3,6-tetrahydropyridine (MPTP) toxin one hour before sacrificing them to induce acute oxidative stress, but no cell death [3]. Brains were serially fractionated, and parkin distribution was quantified across soluble and insoluble compartments. There, we measured a decrease of murine parkin in the soluble fraction and a corresponding rise in the insoluble fractions of MPTP- vs. saline-injected littermates (Fig. 2f, g).

In the second *in vivo* model, we observed a similar, significant shift in parkin distribution toward insolubility in adult mice that were haploinsufficient for the *Sod2* gene, which encodes mitochondrial MnSOD, and which occurred in the absence of an exogenous toxin (Fig. 2h, i). Of note, in both models we confirmed the expected rise in H₂O₂ levels (see below and El-Kodsi et al. [17]). Moreover, in contrast to murine parkin, the solubility of



endogenous Dj-1, which is encoded by a second, ARPD-linked gene, was not visibly altered under these elevated oxidative stress conditions, as monitored by SDS/PAGE/Western blotting (Fig. 2h).

Parkin is reversibly oxidized in the adult human brain

The correlation between parkin insolubility and H₂O₂ levels in the human brain suggested to us that the relation could be

Fig. 2 Decline in parkin solubility correlates with a rise of oxidative stress in mammalian brain. **a** Mean concentrations of H_2O_2 in human brain cortices grouped by age range, as described in Fig. 1. Individual data points represent separate brains, as reported in Supplementary Table 1, online resource. Results are plotted as mean \pm SEM; significance was determined using 2-way ANOVA [$F(2, 76)=26.21$, $p<0.001$] with Tukey's post hoc test (** $p<0.01$; *** $p<0.001$). **b–c** Linear regression analysis of H_2O_2 concentrations in control cortices ($\mu\text{M/g}$ tissue) as a function of age (**b**), and **c** linear regression analysis of parkin solubility as a function of H_2O_2 levels in the same specimens ($n=22$). Red circles denote three disease cortices (non-*PRKN*-linked parkinsonism). H_2O_2 concentration coefficient (in **c**) was -4.2 (95% CI: -7.92 to -0.48 , $P=0.0287$). **d–e** Western blots (**d**) of parkin distribution in brain lysates of 2–4 month-old wild-type C57Bl/6 J mice containing either saline or 1% H_2O_2 ; **e** parkin signal distribution was quantified using ImageJ, as controlled for respective loading controls, in both soluble and insoluble fractions. A student t-test was used for statistical analysis (* $p<0.05$). **f, g** Western blots **f** of parkin distribution in brains of wild-type C57Bl/6 J mice 1 h following intraperitoneal administration of either saline or MPTP neurotoxin (40 mg/kg); **g** parkin signals were quantified as in **e**. **h–i** Western blots **h** of fractionated brain homogenates from C57Bl/6 J wild-type and *Sod2*[±] mice; **i** parkin signals were quantified and statistically analyzed as in **e** (* $p<0.05$). Note, Western blots shown in this figure followed SDS/PAGE under reducing conditions

due to posttranslational, oxidative modifications. Indeed, in contrast to SDS-containing brain fractions analyzed under reducing conditions (+DTT), when gel electrophoresis was performed under non-reducing (-DTT) conditions, we detected parkin proteins ranging in M_r from >52 to 270 kDa, invariably in the form of redox-sensitive, high molecular weight (HMW) smears (right vs. left panel; Fig. 3a). We saw the same pattern in fractions prepared from control midbrains; no such reactivity was seen in SDS-extracts of parkin-deficient ARPD brains, thus demonstrating the specificity of protein detection.

We confirmed that reversible oxidation of brain parkin was also present in soluble (TS-, TX-) fractions, albeit at lesser intensities (Fig. 3b; data not shown). Of note, the formation of high M_r parkin was not due to secondary oxidation in vitro, because specimens had been processed and fractionated in the presence of iodoacetamide (IAA) prior to SDS/PAGE in order to protect unmodified thiols. These HMW parkin smears also did not arise from covalent ubiquitin-conjugation, such as due to auto-ubiquitylation of parkin, owing to the fact that such adducts cannot be reversed by reducing agents (e.g., DTT) (data not shown).

Because we predicted that the loss of parkin solubility was due to thiol-based, posttranslational oxidation events [50], we first sought to test this in vitro using purified, tag-less, full-length, recombinant (r-) parkin. There, we observed the H_2O_2 dose-dependent formation of HMW smears and loss of parkin solubility; however, r-parkin protein solubility was greatly recovered by adding DTT (Fig. 3c; Supplementary Fig. 3a, online resource) or

β -mercaptoethanol (not shown). Demonstrating its sensitivity to bi-directional redox forces, the exposure of native r-parkin to excess DTT also rendered it increasingly insoluble (Supplementary Fig. 3b, online resource), likely due to loss of zinc-sulfur chelation in its four RING domains [31, 47]. Unlike r-parkin, the addition of up to 1 M DTT in the extraction buffer did not induce parkin's extraction into a soluble phase (i.e., TS- or TX-fractions) in aged human brain tissue (Supplementary Fig. 3c, online resource).

We confirmed by mass spectrometry (MS) of the holoprotein carried out without any trypsin digestion that all 35 cysteine-based thiol groups of human r-parkin are principally accessible to alkylation by IAA (right vs. left panel; Supplementary Fig. 3d, online resource). These results unequivocally demonstrated that each parkin cysteine theoretically possesses the capacity to have its thiol be modified. Nevertheless, in these in vitro experiments we consistently observed a concentration-dependent change in r-parkin solubility, thereby suggesting that some thiols were more amenable than others to modification by reactive species (see below and summary in Supplementary Table 2, online resource).

Oxidative conditions alter parkin structure

The progressive insolubility of brain parkin and r-parkin due to redox stress suggested that the protein had undergone structural changes. Indeed, when we analyzed the effects of spontaneous oxidation using native r-parkin by far-UV-circular dichroism (Fig. 3d), soluble fractions initially contained both α -helically ordered as well as unstructured r-parkin proteins. Five days later, r-parkin preparations were separated by centrifugation and fractions re-analyzed. There, we found a marked shift to increased β -pleated sheet-positive r-parkin in insoluble fractions (Fig. 3d). Similarly, when we monitored r-parkin during spontaneous oxidization using dynamic-light scattering (Supplementary Fig. 3e, online resource), we observed a gradual shift in the hydrodynamic diameter from 5.1 nm, representing a folded monomer, to multiple peaks with larger diameters 5 h later. The latter indicated spontaneous multimer formation, which was partially reversed by the addition of DTT (right panel; Supplementary Fig. 3e, online resource). Thus, these structural and solubility changes of r-parkin were congruent with our immunoblot results for human brain parkin (Fig. 3a).

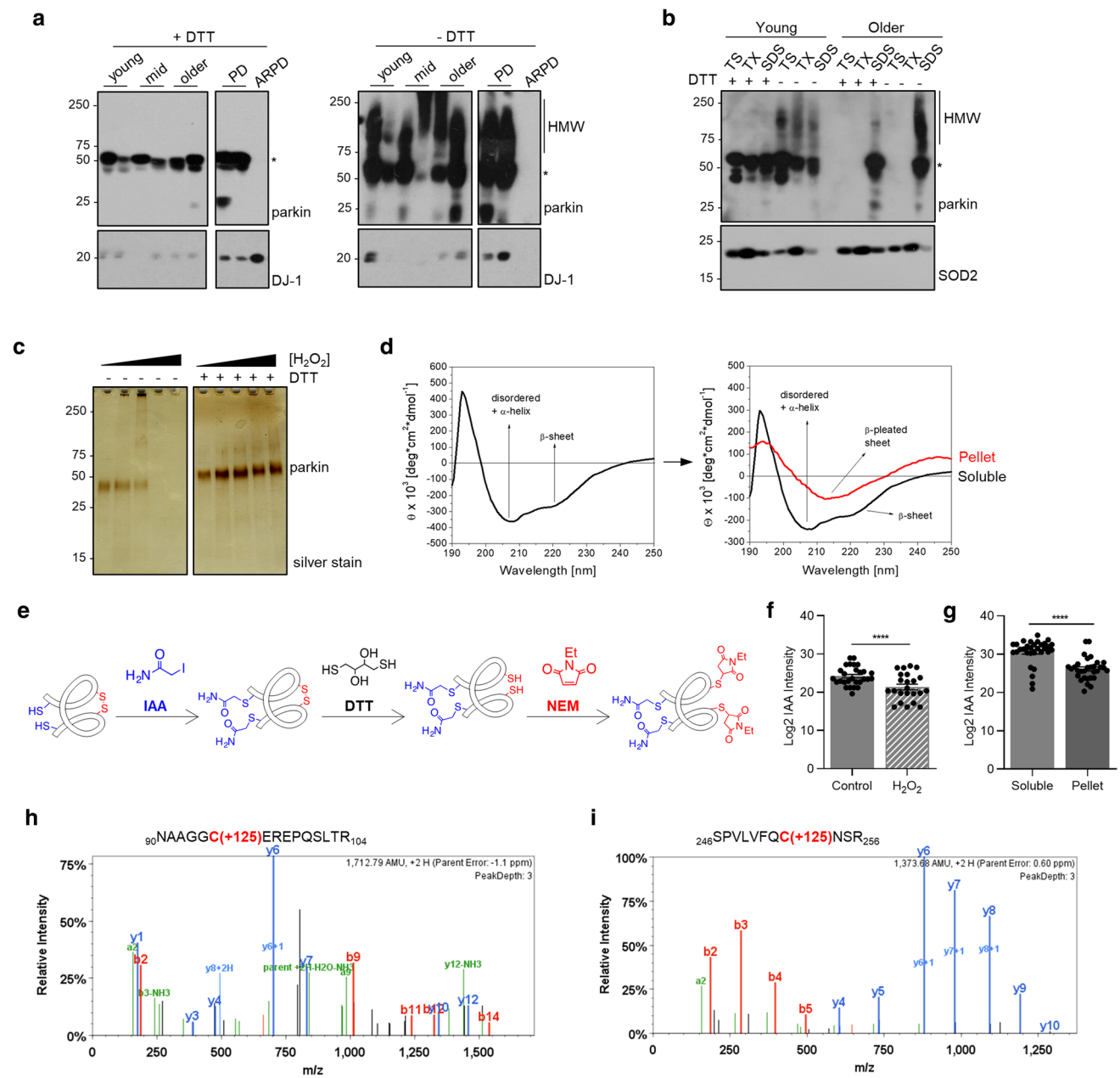


Fig. 3 Parkin's solubility and structure are altered by oxidative modifications. **a** Western blots of parkin and DJ-1 in SDS fractions from normal cortices (3 age groups are shown) and two age-matched patients, i.e., idiopathic Parkinson's (PD) and parkin-deficient ARPD. Sister aliquots of the same lysates were processed in parallel by SDS-PAGE either under reducing (+DTT) or non-reducing (-DTT) conditions. **b** Western blots of parkin and SOD2 distribution in serially fractionated human cortices from a young individual (age, 5 years) and an adult (62 years) subject, and separated by SDS-PAGE under reducing (+DTT) and non-reducing (-DTT) conditions. **c** Silver staining of the supernatant of sister aliquots of r-parkin following initial exposure to increasing concentrations of H_2O_2 (0–2 mM) followed by the addition (or absence of) DTT (100 mM) prior to centrifugation as indicated. **d** Circular dichroism spectra of soluble, untreated, wild-type r-parkin at the start of experiment ($T=0$; left panel), and spectra of soluble (black line) and aggregated (red line) states following incubation at 37 °C for $T=5$ days (right panel). **e**

Graphic depiction of strategy for LC-MS/MS-based analysis to identify cysteine oxidation state for untreated and H_2O_2 -treated, parkin species, by using IAA-DTT-NEM fingerprinting to identify reduced cysteines with an iodacetamide (IAA) tag or reversibly-oxidized residues with a *N*-ethylmaleimide (NEM) tag. **f**, **g** Quantitative analyses of IAA-modified cysteines captured by LC-MS/MS for **f** untreated vs. H_2O_2 -exposed, wild-type, human r-parkin, and **g** soluble compared to insoluble (pellet) fractions. Each dot represents the log₂-transformed total IAA-signal intensities of individual cysteines ($n=3$ runs for each). The cysteine pool is shown with the mean \pm SEM; significance $**p < 0.01$, as determined using Student *T*-Test. **h–i** LC-MS/MS-generated spectra following trypsin digestion of labelled, oxidized r-parkin indicating NEM adducts (+125 mass gain) at Cys95 and Cys253; r-parkin was exposed to H_2O_2 , and cysteines labelled as in (e). See Supplementary Table 2, online resource, for a complete list of modified cysteines and oxidizing conditions

Hydrogen peroxide modifies parkin at multiple cysteines

To determine whether the oxidation of cysteines and/or methionine residues caused parkin insolubility, we analysed r-parkin that was treated with and without H₂O₂ and/or thiol-alkylating agents using liquid chromatography-based MS (LC–MS/MS). To differentiate reduced from oxidized cysteines we used a serial thiol-fingerprinting approach, which labelled reduced thiols with IAA, and tagged reversibly oxidized thiols with *N*-ethylmaleimide (NEM) after their prior reduction with DTT (Fig. 3e). The first test was to determine how progressive oxidation affected thiol accessibility. As expected, using the strong alkylating agent IAA on the nascent protein (and trypsin digestion to map individually modified peptides), we confirmed that the majority of parkin cysteines were reactive (Supplementary Fig. 3d; Supplementary Table 2, online resource). Intriguingly, when treating native r-parkin with lower H₂O₂ concentrations, we identified an average of 19 cysteines (54.3%) to be modified; in contrast, higher H₂O₂ concentrations increased this number to 32 cysteines (91.4%). These results suggested progressive unfolding of r-parkin with increasing oxidation (Supplementary Table 2, online resource).

Next, we sought to precisely identify the location of oxidized cysteine residues. Using Scaffold PTM-software, we found a rise in the number of oxidized residues (NEM-Cys, range of 3–26), which was proportional to the increase in H₂O₂ concentrations and appeared to begin in parkin's RING1 domain at three residues, i.e., Cys238, Cys241 and Cys253 (Supplementary Table 2, online resource; Fig. 3i), but also involved Cys95 in its linker domain (Fig. 3h). Furthermore, when quantifying thiol modifications by MaxQuant software [10], we found a significant drop for the number of cysteines in the reduced state (IAA-cysteines) within the H₂O₂-treated samples ($P=0.0016$; Fig. 3f), as expected.

In accordance, when comparing cysteine oxidation events in soluble and insoluble fractions of untreated vs. oxidized r-parkin preparations, the number of IAA-Cys was significantly decreased in the pellets ($P < 0.0001$; Fig. 3g). Of note, modifications at methionine residues did not correlate with r-parkin solubility. These collective results unequivocally demonstrated that H₂O₂-induced oxidation events at cysteine-based thiols are linked to both progressive, structural change and lesser solubility of human r-parkin.

Parkin is also irreversibly oxidized in adult human and mouse brains

We next sought to identify oxidation events at parkin cysteines in vivo by LC–MS/MS. To this end, we examined both cortex-derived, human parkin and brain parkin

isolated from intraperitoneally, MPTP toxin- (vs. saline-) treated mice (Fig. 4). Specimens were processed with IAA during homogenization and fractionation to prevent any oxidation artefacts in vitro. Following immunoprecipitation and gel excision of endogenous parkin at the 50–53 kDa range (an example is shown in Supplementary Fig. 4a, b, online resource), we focused on cysteine mapping and the identification of thiol redox states (Fig. 4a). A graphic representation of theoretically possible, thiol-based redox modifications is provided in Supplementary Fig. 4c, online resource).

In human control cortices ($n=12$ runs; summarized in Fig. 4a), we mapped a mean of 46.8 and 19.4% of parkin's wild-type sequence in the soluble and insoluble fractions, respectively. There, we found cysteines in either a redox reduced state (IAA-alkylated Cys + 57; examples shown in Fig. 4b, d) or in oxidized states (e.g., to sulfonic acid Cys + 48). Irreversible oxidation events in human cortices occurred, for example, at Cys95 (Fig. 4c) and Cys253 (Fig. 4e). The relative frequencies of detection for parkin thiols that were found in a reduced state in vivo (and thus, were alkylated by IAA in vitro) in the soluble vs. insoluble fractions of the human brain were 67.3 vs. 38.1%, respectively (Fig. 4a).

Likewise, in saline- and MPTP-treated mouse brains ($n=6$ runs), we mapped 25.0 and 51.5% of wild-type parkin, respectively (summarized in Fig. 4a). Interestingly, akin to the findings in the human brain, we identified the murine sequence-corresponding residue Cys252 in either a reduced or in irreversibly oxidized states (Fig. 4f, g). As mentioned, mice do not carry a cysteine at residue 95 (for sequence comparison, see below). The relative frequencies of detection for thiols that were in a reduced state in vivo (and thus, alkylated by IAA in vitro) in parkin from saline- vs. MPTP toxin-treated mouse brains were 92.9 vs. 68.2%, respectively (Fig. 4a). These collective results demonstrate that parkin cysteines are variably oxidized in adult mammalian brain.

Parkin thiols reduce hydrogen peroxide in vitro

A typical redox reaction involves the reduction of an oxidized molecule in exchange for the oxidation of the reducing agent (examples are shown in Supplementary Fig. 4c, online resource). We, therefore, asked whether parkin oxidation resulted in a reciprocal reduction of its environment (Fig. 5; Supplementary Fig. 5, online resource). Using r-parkin, we established that parkin could reduce H₂O₂ levels in a concentration-dependent manner in vitro (Fig. 5a; Supplementary Fig. 5h, online resource). This reducing activity was not enzymatic, in that it did not mirror the dynamics of catalase, and r-parkin did not possess peroxidase activity (Fig. 5a; Supplementary Fig. 5a, online resource). Rather, the reaction was dependent on parkin's thiol integrity, because pre-treatment with NEM (or IAA) and pre-oxidation of the protein

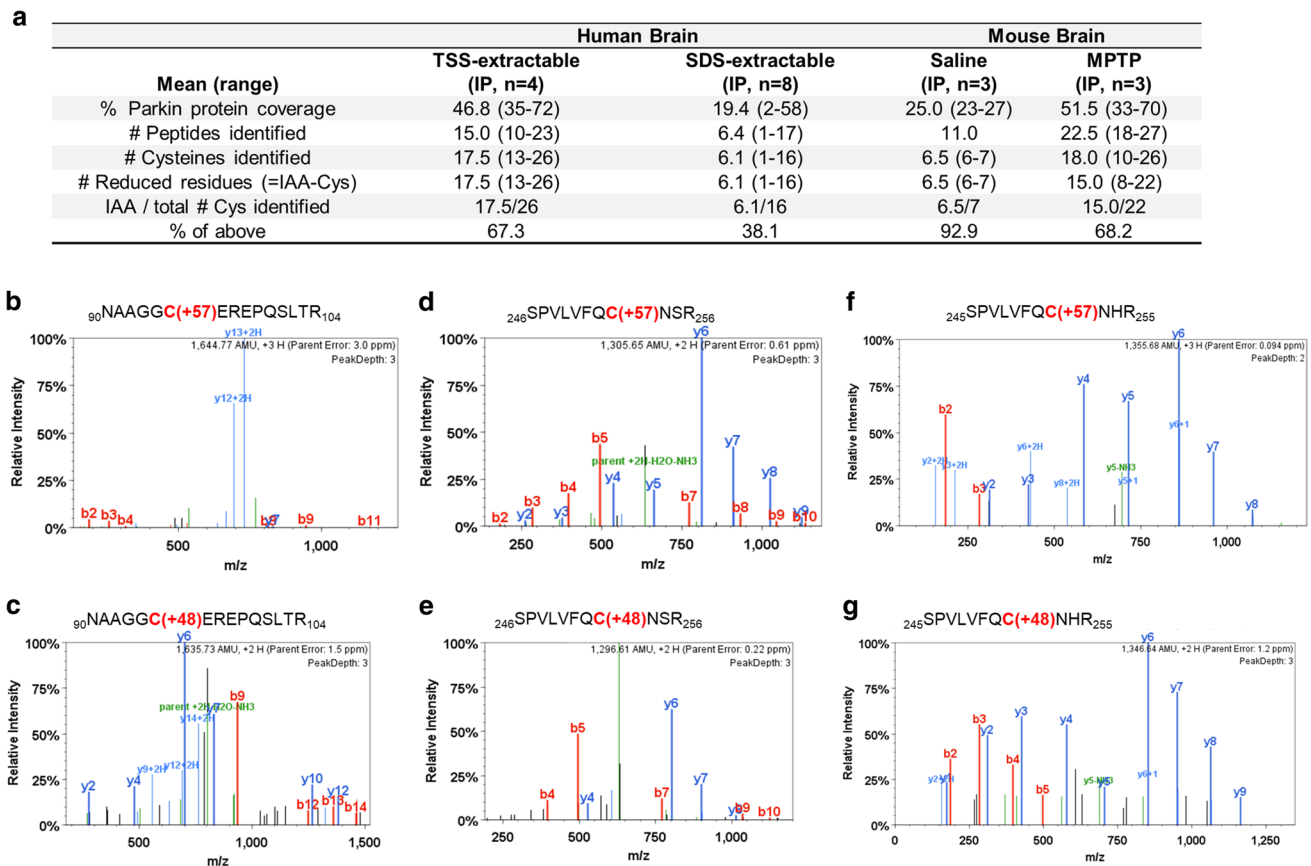


Fig. 4 Select parkin cysteine residues are oxidized in human and mouse brain. **a** Summary of results for 12 immunoprecipitation (IP) runs (TS extracts; $n=4$; SDS extracts, $n=8$) from human cortices and either saline- or acute (1 h) MPTP toxin-treated murine brain (as described in Fig. 2d, e) for endogenous parkin enrichment to identify the redox state of its cysteine residues (see also **b–g**). All

specimens were fractionated in the presence of IAA. **b–g** Among the redox active residues identified Cys95 and Cys253 in human parkin were found in either a reduced redox state (**b, d**) (i.e., IAA-labelled; +57 mass gain) or (**c, e**) in irreversibly oxidized states, e.g., to sulfonic acid (trioxidation; +48 mass). In mouse brain parkin (**f, g**), Cys252 was found either reduced or oxidized as well

with H_2O_2 abrogated the ROS-reducing activity of r-parkin (Fig. 5b; Supplementary Fig. 5b, g, online resource). It thus appeared similar to the effect of glutathione (Fig. 5a; Supplementary Fig. 5a, e, f, online resource).

The anti-oxidant effect by r-parkin was also dependent on its intact Zn^{2+} coordination, because increasing concentrations of the divalent ion chelator, EDTA, abrogated the activity; the latter could be ameliorated by supplementing the reaction buffer with zinc (Supplementary Fig. 5c, online resource). As expected, the exposure of r-parkin to excess H_2O_2 (or excess DTT) led to the release of zinc ions from the nascent recombinant protein, as measured in vitro (Supplementary Fig. 5d, online resource).

Interestingly, RNF43 (a distinct E3 ligase that contains a zinc-finger domain), HOIP (an E3 ligase containing a RING domain) and bovine serum albumin (BSA, which akin to parkin has 35 cysteines), did not show any H_2O_2 -lowering capacity (Fig. 5c, d; Supplementary Fig. 5e, online resource). Further, Parkinson's-linked

α -synuclein, which has no cysteines, also had no reducing effect (Fig. 5c, d). These results suggested that the cysteine-rich, primary sequence and the tertiary structure of r-parkin conferred anti-oxidant activity.

We next examined an additional, cysteine-containing, ARPD-linked protein, e.g., r-DJ-1 and two disease-linked variants of full-length r-parkin, p.G328E and p.C431F, as well as a C-terminal RING2-peptide of parkin (r-parkin_{321C}). We also used a second ROS quantification assay for further validation and to expand our dose-dependency studies (Fig. 5e, Supplementary Fig. 5f–m, online resource). There, r-DJ-1 and r-parkin_{321C} showed negligible H_2O_2 -lowering capacity, and the two point-mutants conferred less activity than did wild-type, human r-parkin (Fig. 5e). As expected from typical redox reactions (Supplementary Fig. 4c, online resource), the lowering of ROS in vitro correlated with reciprocal r-parkin oxidation, as revealed by SDS/PAGE, which was performed under

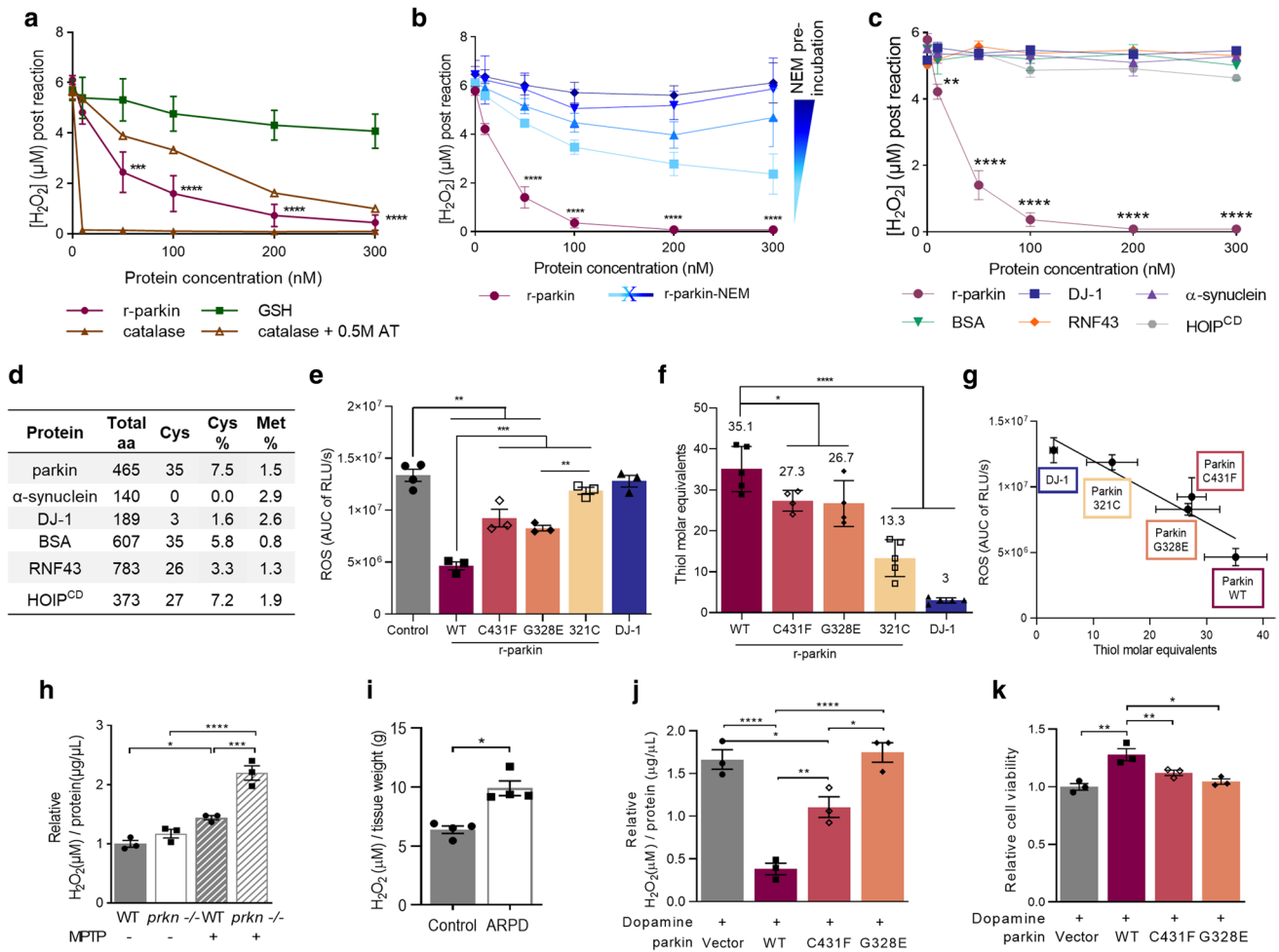


Fig. 5 Wild-type parkin lowers hydrogen peroxide in vitro, in cells and the brain. **a–c** Quantification of H_2O_2 concentration using AmplexRed, demonstrating **(a)** full-length, human, recombinant (r-) parkin when incubated with H_2O_2 is able to reduce it in a r-parkin concentration-dependent manner. Effects of r-Parkin were compared to catalase and GSH at equimolar concentrations as well as following partial inhibition of catalase by amino-triazole (AT), as indicated. **b** Pre-incubation of r-parkin with a thiol-conjugating compound (NEM) inhibits parkin-dependent H_2O_2 reduction in a NEM-concentration-dependent manner. **c** Reducing capacity of wild-type r-parkin compared to two other, PD-linked proteins (DJ-1; α -synuclein), bovine serum albumin (BSA) and two RING-carrying ubiquitin ligases (RNF43; HOIP^{cd}, cd=catalytic domain). Their respective cysteine and methionine contents are summarized in **(d)**. Two-way ANOVA with Tukey's post hoc test (** $p < 0.01$, *** $p < 0.001$, and **** $p < 0.0001$) was used for statistical analysis **a** [$F(15, 48) = 5.069, p < 0.0001$]; **b** [$F(20, 60) = 3.966, p < 0.0001$]; and **c** [$F(25, 72) = 22.91, p < 0.0001$]. **e** Area under the curve (AUC) plots for results from in vitro colorimetric assays, where AUC integrates total H_2O_2 levels measured over the time course of the assay (see also Supplementary Fig. 5f, online resource). Comparison of WT r-parkin with DJ-1, two r-parkin point mutants, and r-parkin_{321–465} (321C). Results represent $n = 3 \pm SD$ using one-way ANOVA [$F(7, 17) = 99.87, p < 0.0001$] with Tukey's post hoc test * $p < 0.05$,

** $p < 0.01$, *** $p < 0.001$, and **** $p < 0.0001$. **f** Quantification of reactive thiol content (in molar equivalents) for r-parkin (WT; two point mutants; 321C) and full-length r-DJ-1 using the Ellman's reagent assay. Results analyzed by one-way ANOVA [$F(4, 18) = 45.11, p < 0.0001$]. **g** Correlation curve between number of free thiols **(f)** vs. the H_2O_2 -reducing capacity **(e)** for indicated proteins with $R^2 = 0.8789$. **h–i** Quantification of H_2O_2 levels in **(h)** saline vs. MPTP toxin-treated *prkn* wild-type (WT) and *prkn*^{-/-} mouse brain ($n = 3$ /genotype/condition), and **i** in human brain from parkin-deficient ARPD cortices compared to age- and *post-mortem* interval-matched controls ($n = 4$ /group) collected at the same institution. Results are represented as the mean concentration of H_2O_2 (μM) per total protein concentration ($\mu g/\mu L$) or tissue weight (g) analyzed $\pm SEM$; * $p < 0.05$, *** $p < 0.001$, and **** $p < 0.0001$ determined using a Student *T*-test or one-way ANOVA with Tukey's post hoc test; [$F(3, 8) = 45.41, p < 0.0001$]. **j, k** H_2O_2 quantification **(j)** and cell viability assay **(k)** for dopamine-treated, human M17 cells expressing either WT or two ARPD-linked parkin point mutants, as indicated relative to treatment with vehicle alone. Cells were exposed to 200 μM dopamine or vehicle for 20 h, as indicated. Data points represent the mean of duplicates $\pm SEM$ ($n = 3$ experiments); * $p < 0.05$ and ** $p < 0.01$, and **** $p < 0.0001$ by one-way ANOVA with Tukey's post hoc test: **j** [$F(3, 8) = 35.34, p < 0.0001$]; and **k** [$F(3, 8) = 12.92, p = 0.0020$]

non-reducing conditions immediately after the reaction with H_2O_2 (Supplementary Fig. 5n, online resource).

These results suggested that the anti-oxidant activity by r-parkin was dependent on its reactive thiol content, which we examined next using the Ellman's reagent. There, full-length r-parkin, r-parkin_{321C} and r-DJ-1 showed the predicted number of reactive thiols, whereas the single point-mutant variants of r-parkin revealed fewer accessible thiols (Fig. 5f). From these results, we observed a linear correlation between thiol equivalencies and the degree of ROS reduction in vitro, demonstrating that a greater number of readily reactive and/or a greater number of accessible thiols in human parkin proteins corresponded with a more effective lowering of H_2O_2 (Fig. 5g).

Hydrogen peroxide levels are increased in parkin-deficient brain

To explore whether parkin oxidation conferred ROS reduction in vivo, we first quantified H_2O_2 concentrations in the brains of wild-type and *prkn*^{-/-} mice. A trend, but no significant difference, was measured under normal redox equilibrium conditions. However, when analyzing brain homogenates from mice treated with MPTP-toxin vs. saline, carried out as above (Fig. 2), we found significantly higher H_2O_2 levels in the brains of adult *prkn*^{-/-} mice compared to wild-type littermates ($P < 0.001$; Fig. 5h). Similarly, in adult humans H_2O_2 levels were significantly increased in the cortex of *PRKN*-linked ARPD patients vs. age-, PMI-, ethnicity- and brain region-matched controls [42] ($P < 0.05$; Fig. 5i). Specimens of three non-*PRKN*-linked patients with parkinsonism showed H_2O_2 levels comparable to those from age-matched normal cortices (Fig. 2b, red circles). We concluded that the expression of wild-type *PRKN* alleles contributes to the lowering of ROS concentrations in adult, mammalian brain.

Parkin prevents dopamine toxicity in cells in part by lowering hydrogen peroxide

To address the question of selective neuroprotection, we revisited the role of parkin in cellular dopamine toxicity studies [51, 104]. We first tested parkin's effect on ROS concentrations in dopamine-synthesizing, human M17 neuroblastoma cells. There, dopamine exposure of up to 24 h caused a significant rise in endogenous H_2O_2 ($P < 0.05$; Fig. 5j), as expected. Wild-type *PRKN* cDNA expression effectively protected M17 cells against the dopamine stress-related rise in H_2O_2 levels ($P < 0.0001$; Fig. 5j). By comparing sister cultures that expressed similar amounts of exogenous parkin proteins, the E3 ligase-inactive p.C431F mutant had a partial rescue effect, whereas p.G328E, which we confirmed to retain its E3 ligase activity in vitro, showed

no H_2O_2 -lowering capacity in these cells (Fig. 5j; and data not shown).

Moreover, only wild-type parkin, but none of the mutant variants tested, increased the viability of M17 cells under rising dopamine stress conditions ($P < 0.01$; Fig. 5k; and data not shown). This protective effect also correlated with parkin insolubility and its HMW smear formation, as expected from previous studies [51]. These posttranslational changes in M17-expressed parkin were not reversible by DTT or SDS (Supplementary Fig. 6a, b, online resource), thereby suggesting irreversible dopamine-adduct formation. Notably, the protection from dopamine toxicity positively correlated with the level of *PRKN* cDNA transcribed, as confirmed in sister lines of M17 cells that stably express human, wild-type parkin. There, we estimated that ~4 ng of parkin protein expressed in healthy, neural cultures neutralized each μM of dopamine added during up to 24 h (Supplementary Fig. 6c, d, online resource).

Parkin binds dopamine radicals predominantly at primate-specific cysteine 95

We next explored which thiols of parkin were involved in the neutralization of dopamine radicals. Covalent conjugation of RES metabolites at parkin residues had been previously suggested [51, 104], but not yet mapped by LC-MS/MS examining the whole protein. Aliquots of r-parkin were exposed to increasing levels of the relatively stable dopamine metabolite aminochrome. As expected, this led to the loss of protein solubility and HMW species formation at the highest dose tested (Fig. 6a, b). These reaction products were then used to map modified residues by LC-MS/MS. Specifically, proteins corresponding to r-parkin monomer (51–53 kDa) and two HMW bands, one at ~100 kDa, the other near the loading well, were gel-excised (Fig. 6a), trypsin digested and analyzed.

There, we made the following four related observations: (i) Increasing aminochrome concentrations led to a significant decline in the total number of spectra readily identified by LC-MS/MS as parkin-derived peptides, both in the monomeric and HMW bands ($P < 0.001$ and $P < 0.0001$), respectively (Fig. 6c). This indicated to us either a marked loss in solubility (and thus, lesser accessibility by trypsin) or a rise in heterogeneous, complex modifications, which rendered the analyte undetectable by LC-MS/MS, or both; (ii) Despite fewer spectra recorded, we identified a significant increase in the number of oxidized cysteines (such as irreversibly modified to sulfonic acid) following aminochrome exposure, in particular within the HMW bands of r-parkin ($P < 0.0001$; Fig. 6d); (iii) Under these conditions, four distinct forms of dopamine metabolites were found conjugated to parkin cysteines. Mass shifts of +145, +147, +149 and +151 were identified, which represented covalent

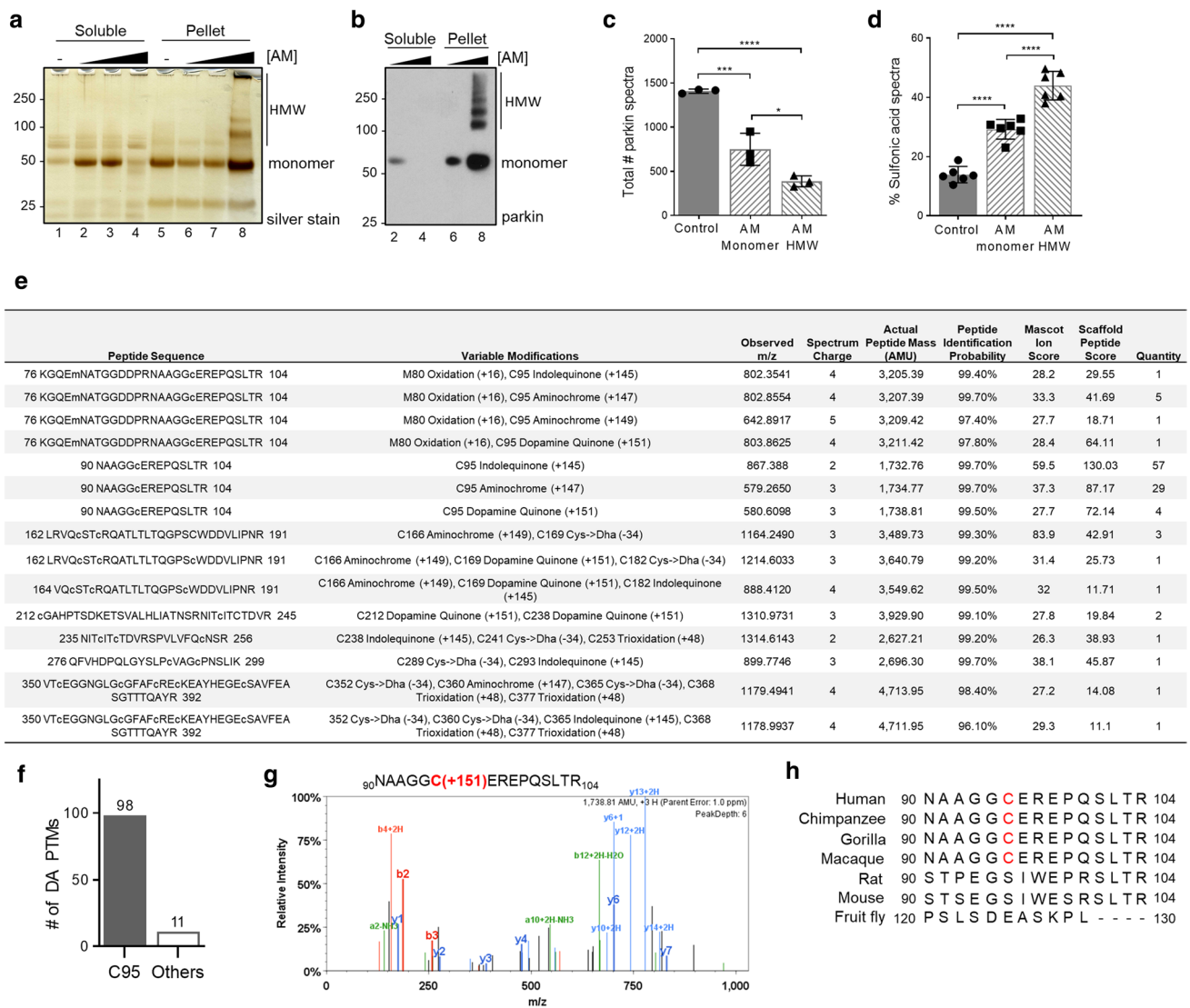


Fig. 6 Human parkin conjugates dopamine radicals foremost at residue Cys95. **a, b** Silver staining (**a**) and Western blot (**b**) of r-parkin in soluble (supernatant) and insoluble (pellet) phases following exposure to increasing concentrations of aminochrome (AM; 0–200 μ M) and analyzed under non-reducing conditions. See lane number for corresponding samples. **c** Mean total number of parkin spectra, as identified by LC–MS/MS following trypsin digestion, of control vs. monomeric vs. high molecular weight (HMW), AM-modified r-parkin. Data represent the mean of $n=3$ runs \pm SEM. * $p<0.05$; *** $p<0.001$; **** $p<0.0001$ by one-way ANOVA with Tukey's post-hoc test [$F(2,6)=64.73$, $p<0.0001$]. **d** Percentage of peptides carrying a sulfonic acid modification in control vs. monomeric and HMW, AM-modified r-parkin. Each point represents one gel specimen submitted to MS. The percentage was calculated using only the subset of peptides that were ever detected as carrying a sulfonic acid modification. Statistics were done as in (**c**) [$F(2,15)=96.87$,

$p<0.0001$]. **e** Table summarizing LC–MS/MS-based detection of adducts representing dopamine metabolites conjugated to cysteines identified in human r-parkin following exposure to aminochrome in vitro. Chemical structures for identified cysteine-conjugated adducts are shown in Supplementary Fig. 7b, online resource. Individual quantification of each peptide with adduct listed is shown on the right side of the table. **f** Frequency of occurrences for dopamine-metabolite adducts being detected on Cys95 vs. all other cysteine residues, as detected by LC–MS/MS and individually shown in (**e**). **g** LC–MS/MS-generated spectrum following trypsin digestion of AM-exposed r-parkin highlighting a dopamine (+151 mass gain) adduct covalently bound to Cys95. See also Supplementary Fig. 7c–p, online resource, for additional spectra. **h** Species comparison for wild-type parkin proteins covering sequence alignment of aa90–104, with primate-specific residue Cys95 highlighted in red

attachment by indole-5,6-quinone, two variants of aminochrome (O=; HO–), and dopamine quinone itself, respectively (Fig. 6e; Supplementary Fig. 7a, online resource); and (iv) Unexpectedly, we identified in Cys95 the most

frequently dopamine-conjugated parkin residue ($P<0.0001$; $n=98$ spectra; Fig. 6e–g; Supplementary Fig. 7b–g, online resource). Other residues of r-parkin, which we identified to carry any one of the dopamine metabolites we tracked,

included Cys166, Cys169, Cys182, Cys212, Cys238, Cys293, Cys360 and Cys365, but at a much lesser frequency (Fig. 6e, f; Supplementary Fig. 7h–o, online resource). No dopamine metabolite-related mass shifts were detected in the control samples that had not been exposed to aminochrome, as expected. We noted with interest that residue Cys95 of wild-type parkin, as the most frequently catalogued one to be modified by dopamine metabolites, is also primate sequence-specific (Fig. 6g, h).

Parkin augments melanin formation in vitro, which involves residue cysteine 95

The oxidation of dopamine in the presence of cysteine-containing proteins, which generates covalent adduct-carrying

proteins, underlies structural characteristics during the formation of neuromelanin pigment in the human mid-brain (and pons), of which biochemical aspects have been modeled ex vivo [18, 19]. Given the observed relations between r-parkin, dopamine radical conjugation, aggregate formation and protein insolubility, we next examined whether melanin formation was altered by the presence of parkin. Indeed, wild-type r-parkin augmented total melanin formation in a protein concentration- and time-dependent manner in vitro (Fig. 7a). Like the wild-type protein, two ARPD-linked, full-length r-parkin variants, p.C431F and p.G328E, also augmented melanin formation in vitro, when monitored over 60 min, whereas r-DJ-1 and BSA showed no effect under these conditions (Fig. 7b).

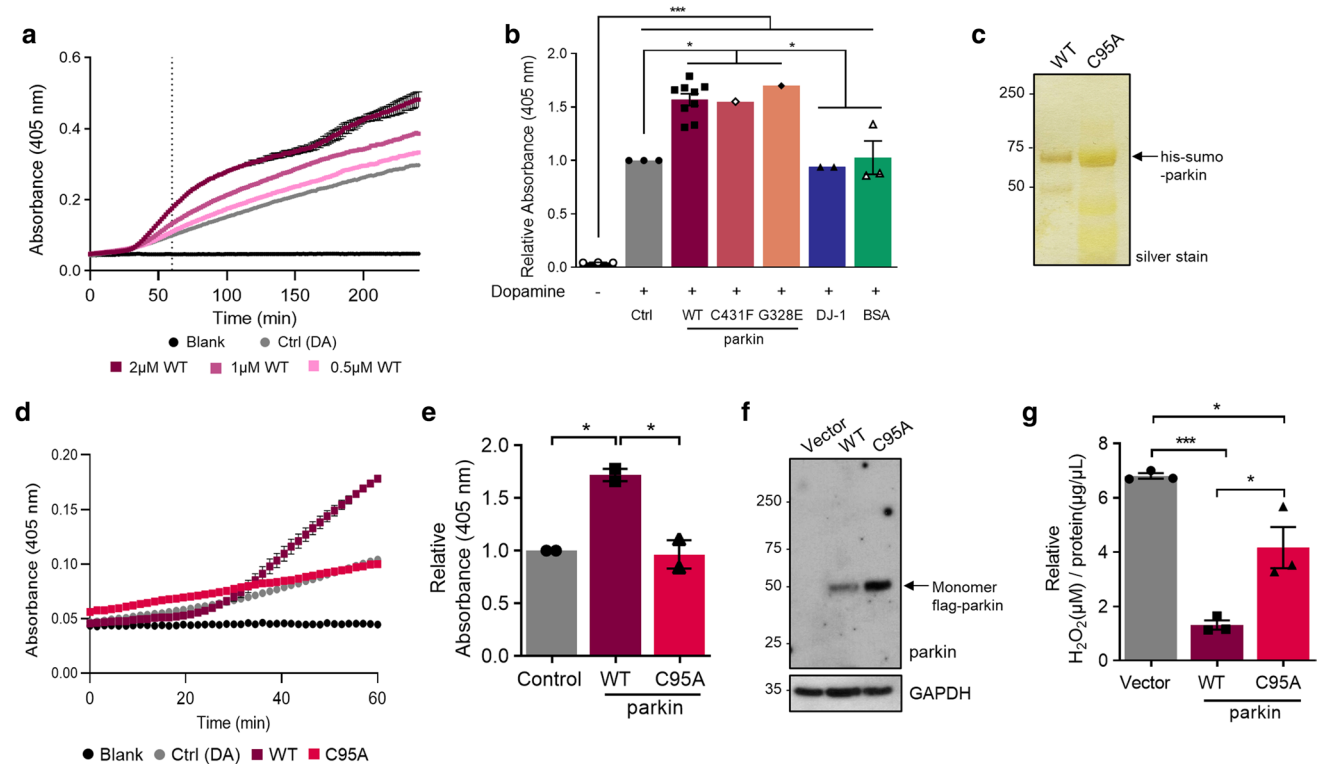


Fig. 7 Parkin-dependent increase in melanin formation involves residue cysteine 95. **a** Kinetic curve of melanin production (read at absorbance 405 nm) over time in the absence of exogenous protein (dopamine (DA Ctrl) alone) vs. increasing molar concentrations of wild-type (WT), full-length human r-parkin shown for three concentrations (0.5, 1, 2 μ M). Each condition was performed in triplicate. **b** Total melanin formation for indicated recombinant proteins at 60 min, as expressed relative to its production under dopamine only control (Ctrl) condition. Data represent the mean of triplicates \pm SEM. *** p < 0.05 by 1-way ANOVA with Tukey's post-hoc test [$F(6,15) = 40.05$, p < 0.0001]. **c** Silver gel for the analysis of His-SUMO-tagged, full-length, human r-parkin proteins of wild-type sequence and its variant carrying a p.C95A mutation. SDS/PAGE was performed under reducing conditions. **d**, **e** Representative kinetic curve for melanin production (**d**) and relative total melanin formation

at 60 min (**e**), where production in the presence of wild-type (WT) or p.C95A mutant r-parkin (each, 2 μ M) is shown relative to dopamine (DA) (Ctrl) alone. Data represent mean of $n=2$, each performed in triplicate \pm SEM. *** p < 0.05 by 1-way ANOVA with Tukey's post-hoc test [$F(2,3) = 24.96$, $p = 0.0135$]. **f**, **g** Protein expression, as shown by Western blotting (**f**), and fold change in H_2O_2 levels (**g**) for dopamine-treated M17 cells -relative to vehicle-treated sister wells- that transiently express either flag-control, or WT vs. p.C95A-mutant human parkin-encoding cDNA plasmids. Results are shown as mean \pm SEM ($n=3$) and all dopamine-treated samples (200 μ M dopamine) were normalized to their respective untreated samples. Anti-GAPDH immunoblotting served as a loading control (in **f**). A one-way ANOVA with Tukey's post hoc test (* p < 0.05 and *** p < 0.001) was used for statistical analysis; [$F(2,6) = 36.86$, $p = 0.0004$]

Interestingly, mutagenesis of residue Cys95 to alanine (p.C95A; Fig. 7c), which was confirmed by nucleotide- and protein sequencing (by LC–MS/MS), completely abrogated the enhancing effect by r-parkin on the polymerization rate of dopamine to melanin (Fig. 7d, e). Of note, in our study all the recombinant proteins heretofore analyzed were used after their N-terminal His-SUMO-tag had been removed; however, the p.C95A-mutant was resistant to enzymatic digestion of the tag from the parkin holoprotein. Therefore, both His-SUMO-r-parkin and His-SUMO-p.C95A were utilized (Fig. 7c–e). Importantly, in parallel experiments we saw no difference in the kinetics of melanin formation between wild-type r-parkin proteins that either carried a His-SUMO-tag or were tag-less (not shown). We concluded that under these in vitro conditions, residue Cys95 was highly relevant to enhanced melanin polymerization by human parkin.

Furthermore, when the p.C95A-variant of parkin was expressed in M17 cells and examined in our dopamine toxicity assay, the mutant protein showed only a partial effect in H₂O₂ lowering capacity when compared to wild-type parkin, even when p.C95A was expressed at much higher levels (Fig. 7f, g). These results were consistent with our collective LC–MS/MS results of oxidative modifications of parkin at Cys95 (shown in: Figs. 3h, 4c; Supplementary Table 2, online resource). We reasoned from these complementary ex vivo results that wild-type parkin could be associated with the synthesis of neuromelanin in vivo. Therefore, we sought to explore this further in dopamine neurons of human midbrain.

Anti-parkin reactivity localizes to neuromelanin in the *Substantia nigra* of adult control brain

Subcellular localization studies of parkin in human brains had previously been hindered by the lack of renewable antibodies (Abs) that reliably detect the protein in situ [73, 77, 81, 85]. We, therefore, developed and extensively characterized several, monoclonal Abs of the IgG₂b-subtype using preparations of untagged, full-length, human r-parkin as immunogen. To this end, we generated four stable, epitope-mapped clones, i.e., A15165B, A15165D, A15165G, and A15165E. The performance and specificity of these clones had been confirmed by ELISA, dot blot analyses, SDS/PAGE/Western blotting under reducing conditions, which included the usage of ARPD brain extracts, immunoprecipitation from the human brain and indirect immunofluorescence in cellular studies (Supplementary Fig. 8a–c, online resource; Tokarew et al., manuscript in preparation). Importantly, clones A15165D, A15165G, and A15165E were able to specifically detect human parkin in human brain sections by immunohistological methods (see below).

Serial sections of adult, human midbrain from control subjects were developed by traditional

immunohistochemistry (IHC) using metal-enhanced 3–3'-diaminobenzidine (eDAB), which generates a black signal for positive immunoreactivity. There, anti-parkin clones A15165D, A15165G and A15165E revealed dark, granular staining throughout the cytoplasm of pigmented cells (ages, ≥ 55 years) (Fig. 8a, b, d). Using sections of anterior midbrains from nine adult control subjects, ≥ 83% of the anti-tyrosine hydroxylase (TH)-positive neurons were also positive for parkin, as quantified by double labelling (Fig. 8c). Under these conditions and Ab concentrations, no anti-parkin signal was generated by clone A15165B, which had been successfully used in IP experiments above (Fig. 4a). Further, in brainstem nuclei outside the *S. nigra*, for example in neurons of cranial nerve III (CNIII) and the periaqueductal grey, as well as in sections of control cortices anti-parkin clones A15165D, -G and -E also stained vesicular structures adjacent to the nucleus, albeit at a much lesser intensity than pigmented neurons (Tokarew et al., manuscript in preparation).

Intriguingly, sections from younger control subjects (ages, ≤ 33 years) that were processed in parallel revealed less intense, anti-parkin reactivity in *S. nigra* neurons, which matched the paucity of their intracellular pigment (Fig. 8e); of note, mature neuromelanin consistently generates a brown color in sections developed without any primary Ab. The different immunoreactivities seen between younger vs. older midbrains suggested that the three anti-parkin clones (A15165D, -G and -E) likely reacted with an age-related, modified form of parkin in situ, because the *PRKN* gene is already expressed in dopamine cells at a young age (Fig. 1b; Supplementary Fig. 1a–d, online resource).

To confirm the specificity of the new anti-parkin clones, we serially stained midbrain sections from a 71 year-old, male ARPD patient, who was entirely deficient in parkin protein due to compound heterozygous deletions of *PRKN* exons 2 and 3 (Fig. 8f; Supplementary Fig. 9a–c, online resource) [38]. Development of serial sections with anti-parkin clones A15165E, -D and -G revealed no immunoreactivity in surviving midbrain neurons of the *S. nigra* from this ARPD subject. In the absence of parkin, there was no signal overlap between eDAB reactivity (black color) and either intracellular neuromelanin granules in surviving dopamine cells or with extracellular pigment (brown; Fig. 8f; Supplementary Fig. 9c, online resource). In parallel, development of midbrain sections from individuals with the diagnoses of dementia with Lewy bodies, of non-*PRKN*-linked, sporadic PD as well as of cases with incidental Lewy bodies readily demonstrated eDAB reactivity overlapping with neuromelanin for all three anti-parkin clones (Supplementary Fig. 9d–g, online resource; and data not shown). These results demonstrated that the staining by the three anti-parkin clones in our microscopy studies of *post mortem* human brain appeared specific.

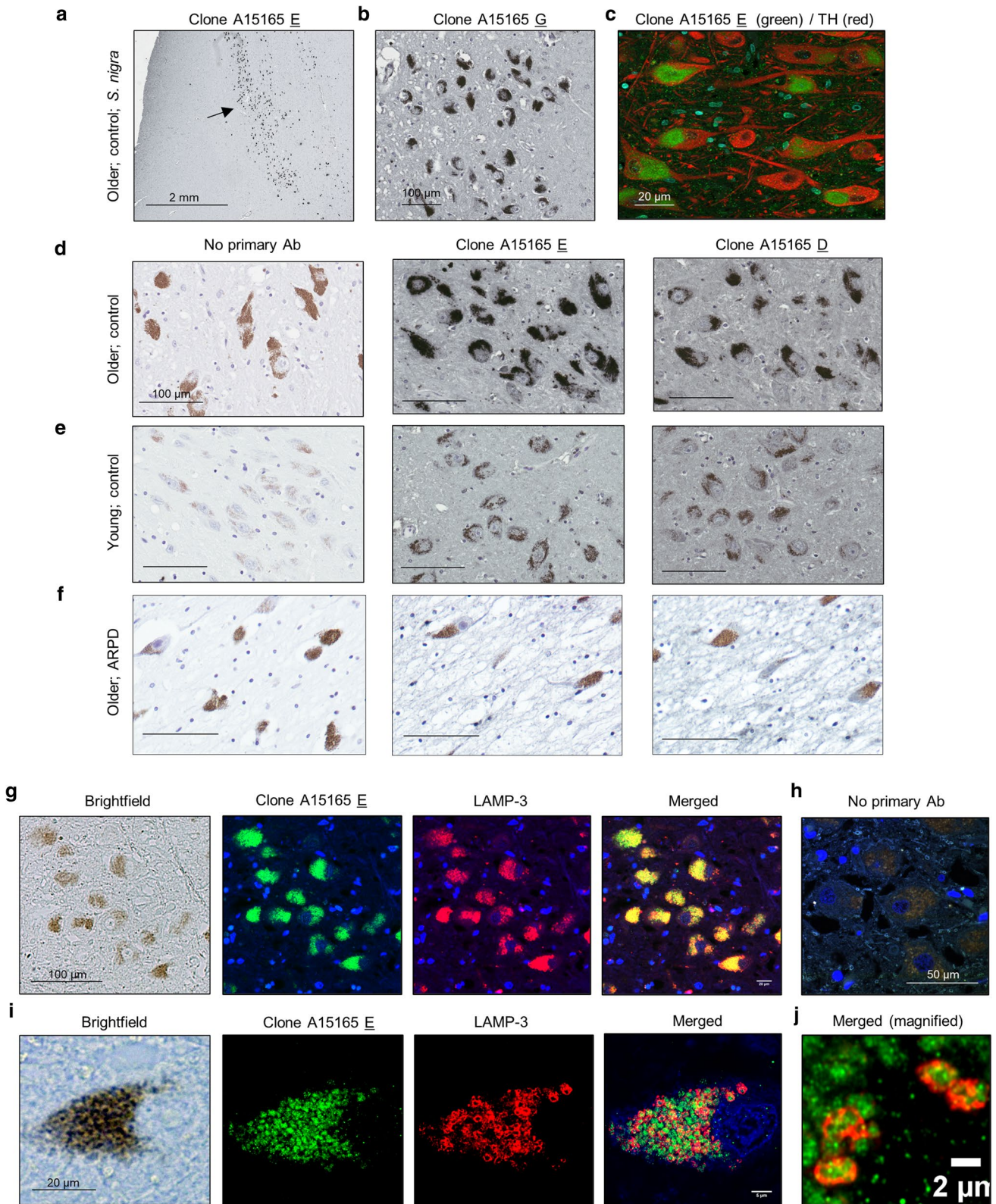


Fig. 8 Parkin localizes to neuromelanin pigment in *S. nigra* neurons of normal human midbrain. **a, b** Immunohistochemical detection of parkin in the adult human brain including dopamine neurons of the *S. nigra* using anti-parkin monoclonal antibody clones A15165E (**a**) and -G (**b**). **c** Double labelling for tyrosine hydroxylase (TH) and parkin (clone A15165E) in the *S. nigra* from an adult control subject using indirect immunofluorescence microscopy. **d–f** Immunohistochemical reactivities generated by no primary antibody vs. two anti-parkin (Clones A15165E, -D) antibodies on sections of the *S. nigra* from two control subjects, aged (**d**) 66 years and (**e**) 24 years, as well as (**f**) from a parkin-deficient ARPD case, aged 71 years. In the indicated panels, immunoreactivity was detected by metal-enhanced DAB (eDAB; generating black colour) and hematoxyline as a counterstain (blue). No primary antibody added generates a pigment-induced signal for neuromelanin (brown). Scale bars represent 100 μm , or as indicated. **g–j** Immunofluorescent signals, as generated by double-labelling of human *S. nigra* sections containing dopamine neurons, using anti-parkin (clone A15165E; green colour) and anti-LAMP-3/CD63 (red colour) antibodies; (blue colour, Hoechst stain). Bright-field microscopy image in the same field (neuromelanin pigment is visible; left panel) and a no primary antibody (**h**) run in parallel are shown. **i** Higher magnification of a single dopamine neuron and (**j**) further magnification for visualization of subcellular signals within a neighbouring dopamine neuron is shown, as indicated

Parkin frequently localizes to LAMP-3⁺-lysosomes within *Substantia nigra* neurons

Neuromelanin granules have been shown to occur in specialized autolysosomes [111]. When screening for colocalization of parkin reactivity with a variety of markers for subcellular organelles in sections of adult control brain, we detected that immunofluorescent signals by anti-parkin (green) and anti-CD63/LAMP-3 (red) antibodies strongly overlapped with pigmented granules of nigral neurons (Fig. 8g–i; see also Supplementary Fig. 9h, online resource).

Using confocal microscopy, we demonstrated that in adult midbrain anti-parkin signals, as generated by clone A15165E, and neuromelanin granules were frequently surrounded by circular, ~2 μm (in diameter)-sized rings of anti-LAMP-3 reactivity (Fig. 8i, j). A z-stack video for the parkin and LAMP-3 co-labelling studies is appended (Supplemental Information_video, online resource). We concluded that in the adult, human midbrain from neurologically healthy controls and in surviving neurons of subjects, who suffer from parkinsonism that is not linked to bi-allelic *PRKN* deletion, a pool of parkin appears physically associated with neuromelanin pigment in close association with juxtannuclear, lysosomal structures.

Discussion

Here, we demonstrate that posttranslational modifications of parkin contribute to its age-related decline in solubility, and in exchange, to redox homeostasis in the human brain. Our study also provides insights into the native processing

of the PD-linked parkin protein in the adult midbrain. Parkin's progressive insolubility in the ageing human brain is relatively unique when compared to other PD-linked proteins and several other cellular constituents, which include mitochondrial proteins. It is also tissue and species-specific. Unlike in the brain, approximately 50% of detectable parkin remain soluble in the spinal cord and in skeletal muscle from aged human subjects, and a comparable loss of parkin solubility is not observed in aged rodent brain and adult monkey cortex (Fig. 1a–d, i; Supplementary Fig. 1d, online resource).

In human control brain, the loss of parkin solubility in *post mortem* tissue correlates with a rise in H_2O_2 concentrations and with age, but not with the subject's sex or the length of PMI (Figs. 1e, j, 2a–c). Although we have analyzed autopsy material with a PMI as short as 2 h (Supplementary Table 1, online resource), in future work we will also extend our efforts to the analysis of specimens removed from living subjects during neurosurgical procedures. Using our cohort of specimens, we found that the transition to parkin insolubility in frontal lobe cortices occurs between the ages of 28 and 42 years (Fig. 1b; Supplementary Fig. 1a–b; Supplementary Table 1, online resource). The age at which parkin transitions in the *S. nigra* will require a larger number of midbrain specimens from young, neurologically normal subjects. While we were unable to assess its solubility in midbrains from subjects younger than 20 years, parkin's relative distribution in adult midbrain specimens matched the results of control cortices (Fig. 1b). Of note, in the brainstem nuclei that we examined (*i.e.*, *S. nigra*; *L. coeruleus*; red nucleus; CN III nucleus; periaqueductal grey), we found that parkin's distribution was not visibly affected by disease state per se (11 control cases vs. 9 neuropathological cases; Fig. 1b; Supplementary Table 1, online resource). However, parkin's total abundance was lower in the *S. nigra* of cases from subjects with various forms of neurodegenerative illnesses, as expected (not shown). In mice, brain parkin showed partial partitioning when oxidative stress had been induced systemically, either acutely or chronically (Fig. 2c–i). In future work, we will examine parkin distribution in larger numbers of brainstem specimens of autopsy material with different neuropathological diagnoses.

In accordance, we demonstrate that a key contributor to parkin insolubility is thiol-oxidation and that the resulting, posttranslational modifications are linked to three protective outcomes: (i) the neutralization of a range of potentially toxic, pro-oxidant radicals (ROS, RES); (ii) the effective lowering of H_2O_2 concentrations, including its direct reduction in vitro; and (iii) the apparent effect that parkin has on dopamine metabolism through Cys95-mediated conjugation of its radicals and enhanced melanin formation. We have modeled parkin's redox chemistry-based function in vitro, in cells and in mice, and provide evidence that these

outcomes are physiologically relevant to the human brain. From these observations, we propose that insoluble parkin represents a functionally important protein of the ageing human brain including the *S. nigra*. Further, our findings integrate the early literature related to parkin mutations and stress-induced modifications vis a vis its insolubility, which included a wide range of complementary investigations [6, 9, 28, 29, 60, 92, 98, 99, 103, 104], such as findings from induced pluripotent stem cell-derived, human dopamine neurons [32, 35, 68]. Our discovery of a function for parkin in redox homeostasis also helps explain seemingly disparate evidence of previous observations made in studies of flies, mice [70, 74] and humans [73].

The reactivity of cysteine thiols is governed by their own redox state as well as by the surrounding electrostatic environment, which includes the charges of neighbouring residues [105]. Unlike parkin, 34 out of 35 cysteines found in BSA are engaged in disulphide bonds [37, 72]. BSA was not able to reduce H_2O_2 , nor did it enhance the formation of insoluble melanin polymers in vitro under these conditions. Two other Zn^{2+} -coordinating, cysteine-containing proteins that we tested, RNF43 and HOIP^{CD} (Fig. 5c), also did not lower H_2O_2 , thus suggesting that select cysteines in parkin have a high affinity for ROS and, as discussed below, RES molecules. When mapping the redox state of parkin cysteines under progressively pro-oxidant conditions in vitro, we found that Zn^{2+} -coordinating residues at its RING domains are not protected from modifications by ROS [56] (Supplementary Table 2, online resource). This observation suggests that oxidative changes of parkin in vivo could occur continuously in the form of a gradient, rather than representing a binary event.

Based on our results, we also estimated the levels of pro- vs. anti-oxidant forces. There, the ratio of H_2O_2 -to-r-parkin (0.1–1.0 mM of H_2O_2 per 1 ng of r-parkin) was within the physiological range of what we had measured for human control brain extracts (i.e., 0.4–6.0 mM of H_2O_2 per 1 ng of parkin). In the latter, H_2O_2 concentrations were calculated to lie between 0.7 and 9.1 mM/mg of tissue (see Supplementary Table 1, online resource). Using semiquantitative Western blotting with aliquots of the same Ab lot (Prk8), parkin concentrations were estimated to be ~1.42 ng/mg brain tissue using r-parkin dilutions as standards; these had been run in parallel with brain lysates of ARPD cortices to demonstrate specificity for the detection of the ~51–53 kDa holoprotein. These estimates represent a first approximation of the concentration of wild-type parkin in the adult human brain; these numbers may need to be revised in the future based on controlling for potentially confounding variables, such as the presence of truncated species and modified forms (not detected by our antibodies), and/or due to marked variability in parkin's turnover rate in different regions of the cortex and between subjects.

As was observed for r-parkin, we also found cysteine residues that were oxidized in parkin proteins after their affinity isolation from human control cortices and mouse brains, including of Zn^{2+} -binding ones. For example, Cys253 (Cys252 in mice), which helps coordinate Zn^{2+} within parkin's RING1 domain, was frequently identified by us as being oxidized (Figs. 3i, 4e, g). We predict that variable modifications of non- Zn^{2+} -coordinating residues in human parkin could induce early, conformational changes in parkin's tertiary structure, such as at Cys95, which is located in the—heretofore structurally understudied—linker region, or Cys59, as positioned in its ubiquitin-like (UbL) domain [17] (see Figs. 6e–h, 7c–g). Such N-terminally located changes could profoundly affect both the structure and function of other domains in wild-type parkin, as has been convincingly delineated in studies of parkin's E3 ligase activity as a readout following modifications at its UbL domain [7, 8, 51, 60, 69, 71, 101, 104, 107] (and reviewed by Yi et al. [108]). Our results do not exclude the possibility that other non-thiol-based, posttranslational modifications alter parkin's solubility, such as phosphorylation at Ser65 [46], or at Ser77 [17], which we found in brains of MPTP-treated mice. Currently, ongoing experiments seek to answer the question as to how structural changes caused by select ARPD-linked parkin mutants, e.g., p.C431F and p.G328E, as determined by far-UV-circular dichroism, dynamic-light scattering and NMR techniques, could alter redox functions in vitro. Their completion will add to our understanding as to how these mutants alter solubility and half-life of nascent parkin proteins in cell-based studies [9, 92].

As mentioned above, *PRKN*-linked ARPD is thought to be pathologically restricted to catecholamine producing cells of the brainstem [15, 40, 45, 53, 55]. Dopamine neurons of the *S. nigra* have unique biophysical properties that lead to high bioenergetic demands and the related rise in oxidative stress [23]. Further, unlike in other animals, dopamine is not completely catabolized in the human brain, and neuromelanin is thought to be essential for the sequestration and long-term storage of its otherwise toxic metabolites [110]. We found parkin to be involved in mitigating two well-established, PD-linked stressors (i.e., ROS; dopamine radicals), which is indirectly supported by our findings in the human brain.

We show that parkin functions as a classical redox molecule that is able to lower H_2O_2 in a thiol-dependent manner. In the absence of wild-type parkin, H_2O_2 concentrations are elevated in the human brain (Fig. 5i), in dopaminergic cells (Fig. 5j, k) and in brains from mice exposed to MPTP-toxin (Fig. 5h). There, acute MPTP exposure not only correlated with a decline in parkin solubility but also with the oxidation of select cysteines (Fig. 4a). Hence, *PRKN* expression contributes to *anti-oxidant activity* in vivo through a net reduction in H_2O_2 levels, which can occur in part through its direct

reduction, as shown by us in vitro (Fig. 5; Supplementary Fig. 5, online resource).

Because both MPTP toxin exposure and *Sod2* gene function affect mitochondrial integrity [12, 20], we reason that redox homeostasis in the cytosol, as coregulated by parkin oxidation, could also indirectly influence the health of mitochondria, in addition to E3 ligase-associated mitophagy (and MITAP). Such a cross-talk between cytosol and mitochondria likely includes glutathione metabolism-linked pathways, in which we and others found parkin cysteines to be involved in as well [11, 17, 25, 34, 79, 89].

A role for *PRKN* expression in the neutralization and sequestration of dopamine metabolites may explain why dopamine synthesizing neurons are at greater risk in humans born with parkin deficiency. Previously, parkin has been shown to be uniquely sensitive to dopamine stress leading to aggregate formation [51, 104] (Supplementary Fig. 6a, b, online resource). In both cells and mice, *prkn* gene expression has been indirectly implicated in the metabolism of this neurotransmitter, in particular under ex vivo conditions, such as induced by high dopamine level-induced stress [25, 34–36, 43, 51] (see also Supplementary Fig. 6c, d, online resource).

Our results, and those by others, suggest that dopamine-mediated stress in neural cells is ameliorated when parkin undergoes irreversible modifications by dopamine metabolites. However, in contrast to current interpretations, which stipulate oxidation by quinones is equal to a loss of parkin activity, we posit that such oxidation is part of parkin's physiological role within post-mitotic cells of the adult brain based on two principal findings. First, we demonstrate that wild-type parkin directly interacts with highly electrophilic dopamine metabolites at specific residues, foremost Cys95 (Fig. 6e–h). This primate-specific cysteine is located within the linker region next to charged residues that impact its electrostatic properties and likely its redox reactivity [24, 105]. In support, we found that in addition to dopamine adduct conjugation, Cys95 is vulnerable to ROS attacks (Figs. 3h, 4b, c), and in parallel studies, is S-glutathionylated when exposed to rising concentrations of oxidized glutathione [17]. Strikingly, we found that Cys95 is not only required for parkin-dependent enhanced melanin formation, but also for participation in effective H_2O_2 reduction in M17 cells during dopamine stress-mediated toxicity (Figs. 6e–g, 7f–g).

Second, our finding that parkin augments melanin formation in vitro, together with our finding that the protein is closely associated with neuromelanin granules within LAMP-3⁺ lysosomes of human brain (Fig. 8g–j; Supplementary Fig. 9h, online resource), suggest a role for parkin in *dopamine metabolism-linked neuroprotection* (Supplementary Fig. 10, online resource). We have noted with interest that several autopsy reports have described lesser

neuromelanin content in surviving neurons of the *S. nigra* in *PRKN*-linked ARPD [22, 27, 30, 95, 106, 109] (Fig. 8f). Intriguingly, variants at the *LAMP3/CD63* locus, as well as of other dopamine metabolism-related genes, e.g., *GCH-1*, have been recently identified as modifiers of susceptibility to late-onset, typical PD [33, 66, 100]. However, proof of the concept that parkin plays an important, contributing role in the formation of neuromelanin in human brain awaits a suitable animal model.

To date, parkin is best known for its function as an E3 ligase and the ubiquitin ligation-dependent involvement in mitophagy. Because ubiquitin-ligating activity occurs via cysteine-mediated trans-thiolation, controlling the cellular redox state and functioning as an E3 ligase may not be mutually exclusive. For example, low concentrations of pro-oxidants, as well as sulfhydration, can activate parkin's E3 activity in vitro [71, 97, 107]. A similar duality in functions, i.e., regulating ubiquitylation and redox state in cells, has been previously described for the sensitive-to-apoptosis gene (SAG) product, also known as RBX2/ROC2/RNF7 [93, 94]. It contains a RING finger, and similar to parkin, was found to form HMW oligomers through oxidation of its cysteines [93, 94]. SAG protein protects cells from oxidative stress in a thiol-mediated manner in addition to functioning as an E3 ligase.

From this analogy, we postulate that parkin's *cytoprotective E3 function* and its role in mitophagy are possibly linked to its soluble form within the cytosol, which could be most important during early developmental stages, such as during organ development [26], in dividing striated muscle cells [80], and in relatively younger, neural cells including glia [89]. In support, Yi et al. recently described a strong correlation between parkin point mutants, their impact on structure and protein stability vs. ubiquitin ligase activity and the degree of mitophagy efficiency [108]. Conversely, redox-based neutralization of radicals by wild-type parkin could be more essential to the sustained health of long-lived, postmitotic cells, e.g., *S. nigra* neurons.

In summary, we have shown that parkin fulfils criteria of a typical redox molecule: the sensing of oxidative (and reducing) stress via its thiols; and the direct, reciprocal redox regulation of its environment, thus conferring protective outcomes. If confirmed by future work, this redox chemistry-based expansion of parkin functions in the ageing human midbrain (Supplementary Fig. 10, online resource) may open the door to testing its anti-oxidant role in related neurodegenerative conditions, such as late-onset, non-*PRKN*-linked PD [13]. Most important, our findings emphasize the need for early identification of persons afflicted by bi-allelic *PRKN* gene mutations for the prioritization of appropriate interventions in the future,

such as via gene therapy [44] and polyvalent, anti-oxidant therapy [78].

Supplementary Information The online version contains supplementary material available at <https://doi.org/10.1007/s00401-021-02285-4>.

Acknowledgements We are grateful for the commitment of patients and their families to participate in autopsy studies. We thank Dr. J. Palacino for creating stable M17 cell lines, Drs. A. Brice and E. Fon for sharing *prkn*-null mice, Dr. B. Madras for providing specimens of cynomolgus brain, Drs. R. Tam, L. Dong, Ms. K. Solti and Ms. H. Boston for technical support, Dr. D. Gibbings for antibodies, Dr. D. Gray for assistance with confocal imaging, Drs. M. Medina and R. R. Ratan for encouragement, Drs. S. Bennett, D. Pratt for discussions, and Drs. H. Lochmueller, M. Rousseaux and past members of the Schlossmacher lab for their suggestions.

Author contributions Study design: JMT, DNEK, PT, JJT, MGS; Writing and Figure preparation: JMT, DNEK, NAL, TKF, MJ, APN, JL, GSS, JMW, GT, PT, JJT, and MGS prepared the initial draft of the manuscript and figures. All authors reviewed and/or edited the manuscript and approved of the submitted versions. Experiments: JMT, DNEK, NAL, TKF, MJ, APN, BO, LW, JK, ACN, QJ, RS, JL, MZ, KRB, AT, XD, LP, GT, BS performed experiments; and CRS, ABW, ET, AH, AP, JAC, provided data, tissue specimens and critical comments. Analysis: JMT, DNEK, JL, TKF, GSS, LP, GT, JMW, PT, JJT, MGS performed data analyses. Study supervision: PT, JJT, MGS. Overall responsibility: MGS

Funding This work was supported by the: Parkinson Research Consortium of Ottawa (J.M.T., D.N.E.K., J.J.T.); Queen Elizabeth II Graduate Scholarship Fund (J.M.T.); Government of Canada [Natural Sciences and Engineering Research Council of Canada (J.K.); Canadian Institutes of Health Research (CIHR) MD/PhD Program (J.M.T., A.C.N.); CIHR Research Grant (G.S.S., A.P.); CIHR Canada Research Chair Program (M.G.S., A.P.); Michael J. Fox Foundation for Parkinson's Research (P.T., J.J.T., L.Z., M.G.S.); The Research Foundation of the Multiple Sclerosis Society of Canada; Progressive Multiple Sclerosis Alliance (A.P.); Hungarian Brain Research Program (G.T.); Utra and Sam Bhargava Family (E.T., M.G.S.); and The Ottawa Hospital (E.T., M.G.S.).

Data and materials availability Original data associated with this study are available in the main text and supplementary figures and tables; additional data will be made available upon request.

Compliance with ethical standards

Conflict of interest Drs. B. O'Nuallain, M. Jin, L. Wang, P. Taylor (or were) employees of BioLegend Inc. (Dedham, MA., USA). The Ottawa Hospital receives payments from BioLegend Inc. related to licensing agreements for immunological reagents related to parkin and α -synuclein. Dr. M. Schlossmacher received travel reimbursements from the Michael J. Fox Foundation for Parkinson's Research for participation in industry summits and consulting fees as well as royalties from Genzyme-Sanofi for patents unrelated to this work. Dr. G. Toth is an employee and a shareholder of Cantabio Pharmaceuticals. Dr. A. Holmgren (deceased) served as chairman and senior scientist at IMCO Corporation Ltd AB, Stockholm, Sweden. No additional, potentially competing financial interests are declared.

Open Access This article is licensed under a Creative Commons Attribution 4.0 International License, which permits use, sharing,

adaptation, distribution and reproduction in any medium or format, as long as you give appropriate credit to the original author(s) and the source, provide a link to the Creative Commons licence, and indicate if changes were made. The images or other third party material in this article are included in the article's Creative Commons licence, unless indicated otherwise in a credit line to the material. If material is not included in the article's Creative Commons licence and your intended use is not permitted by statutory regulation or exceeds the permitted use, you will need to obtain permission directly from the copyright holder. To view a copy of this licence, visit <http://creativecommons.org/licenses/by/4.0/>.

References

1. Aguirre JD, Dunkerley KM, Mercier P, Shaw GS (2017) Structure of phosphorylated UBL domain and insights into PINK1-orchestrated parkin activation. *Proc Natl Acad Sci USA* 114:298–303. <https://doi.org/10.1073/pnas.1613040114>
2. Alcock LJ, Perkins MV, Chalker JM (2018) Chemical methods for mapping cysteine oxidation. *Chem Soc Rev* 47:231–268. <https://doi.org/10.1039/c7cs00607a>
3. Ali SF, David SN, Newport GD, Cadet JL, Slikker W Jr (1994) MPTP-induced oxidative stress and neurotoxicity are age-dependent: evidence from measures of reactive oxygen species and striatal dopamine levels. *Synapse* 18:27–34. <https://doi.org/10.1002/syn.890180105>
4. Barodia SK, Creed RB, Goldberg MS (2017) Parkin and PINK1 functions in oxidative stress and neurodegeneration. *Brain Res Bull* 133:51–59. <https://doi.org/10.1016/j.brainresbull.2016.12.004>
5. Berger AK, Cortese GP, Amodeo KD, Weihofen A, Letai A, LaVoie MJ (2009) Parkin selectively alters the intrinsic threshold for mitochondrial cytochrome c release. *Hum Mol Genet* 18:4317–4328. <https://doi.org/10.1093/hmg/ddp384>
6. Chakraborty J, Basso V, Ziviani E (2017) Post translational modification of Parkin. *Biol Direct* 12:6. <https://doi.org/10.1186/s13062-017-0176-3>
7. Chung KK, Dawson VL, Dawson TM (2005) S-nitrosylation in Parkinson's disease and related neurodegenerative disorders. *Methods Enzymol* 396:139–150. [https://doi.org/10.1016/S0076-6879\(05\)96014-X](https://doi.org/10.1016/S0076-6879(05)96014-X)
8. Chung KK, Thomas B, Li X, Pletnikova O, Troncoso JC, Marsh L et al (2004) S-nitrosylation of parkin regulates ubiquitination and compromises parkin's protective function. *Science* 304:1328–1331. <https://doi.org/10.1126/science.1093891>
9. Cookson MR, Lockhart PJ, McLendon C, O'Farrell C, Schlossmacher M, Farrer MJ (2003) RING finger 1 mutations in Parkin produce altered localization of the protein. *Hum Mol Genet* 12:2957–2965. <https://doi.org/10.1093/hmg/ddg328>
10. Cox J, Mann M (2008) MaxQuant enables high peptide identification rates, individualized p.p.b.-range mass accuracies and proteome-wide protein quantification. *Nat Biotechnol* 26:1367–1372. <https://doi.org/10.1038/nbt.1511>
11. Damiano M, Gautier CA, Bulteau AL, Ferrando-Miguel R, Gouarne C, Paoli MG et al (2014) Tissue- and cell-specific mitochondrial defect in Parkin-deficient mice. *PLoS ONE* 9:e99898. <https://doi.org/10.1371/journal.pone.0099898>
12. Dauer W, Przedborski S (2003) Parkinson's disease: mechanisms and models. *Neuron* 39:889–909. [https://doi.org/10.1016/s0896-6273\(03\)00568-3](https://doi.org/10.1016/s0896-6273(03)00568-3)
13. Dawson TM, Dawson VL (2014) Parkin plays a role in sporadic Parkinson's disease. *Neurodegener Dis* 13:69–71. <https://doi.org/10.1159/000354307>

14. Dhaeze T, Tremblay L, Lachance C, Peelen E, Zandee S, Grasmuck C et al (2019) CD70 defines a subset of proinflammatory and CNS-pathogenic TH1/TH17 lymphocytes and is overexpressed in multiple sclerosis. *Cell Mol Immunol* 16:652–665. <https://doi.org/10.1038/s41423-018-0198-5>
15. Doherty KM, Silveira-Moriyama L, Parkkinen L, Healy DG, Farrell M, Mencacci NE et al (2013) Parkin disease: a clinicopathologic entity? *JAMA Neurol* 70:571–579. <https://doi.org/10.1001/jamaneurol.2013.172>
16. Dong X, Liao Z, Gritsch D, Hadzhiev Y, Bai Y, Locascio JJ et al (2018) Enhancers active in dopamine neurons are a primary link between genetic variation and neuropsychiatric disease. *Nat Neurosci* 21:1482–1492. <https://doi.org/10.1038/s41593-018-0223-0>
17. El Kodsi DN, Tokarew JM, Sengupta R, Lengacher NA, Ng AC, Boston H et al (2020) Parkinson disease-linked parkin mediates redox reactions that lower oxidative stress in mammalian brain. *bioRxiv*. <https://doi.org/10.1101/2020.04.26.062380>
18. Ferrari E, Capucciati A, Prada I, Zucca FA, D'Arrigo G, Pontiroli D et al (2017) Synthesis, structure characterization, and evaluation in microglia cultures of neuromelanin analogues suitable for modeling Parkinson's disease. *ACS Chem Neurosci* 8:501–512. <https://doi.org/10.1021/acschemneuro.6b00231>
19. Ferrari E, Engelen M, Monzani E, Sturini M, Giroto S, Bubacco L et al (2013) Synthesis and structural characterization of soluble neuromelanin analogs provides important clues to its biosynthesis. *J Biol Inorg Chem* 18:81–93. <https://doi.org/10.1007/s00775-012-0951-7>
20. Flynn JM, Melov S (2013) SOD2 in mitochondrial dysfunction and neurodegeneration. *Free Radic Biol Med* 62:4–12. <https://doi.org/10.1016/j.freeradbiomed.2013.05.027>
21. Ge P, Dawson VL, Dawson TM (2020) PINK1 and Parkin mitochondrial quality control: a source of regional vulnerability in Parkinson's disease. *Mol Neurodegener* 15:20. <https://doi.org/10.1186/s13024-020-00367-7>
22. Gibb WR, Narabayashi H, Yokochi M, Iizuka R, Lees AJ (1991) New pathologic observations in juvenile onset parkinsonism with dystonia. *Neurology* 41:820–822. <https://doi.org/10.1212/wnl.41.6.820>
23. Giguere N, Pacelli C, Saumure C, Bourque MJ, Matheoud D, Levesque D et al (2018) Comparative analysis of Parkinson's disease-associated genes in mice reveals altered survival and bioenergetics of Parkin-deficient dopamine neurons. *J Biol Chem* 293:9580–9593. <https://doi.org/10.1074/jbc.RA117.000499>
24. Gladkova C, Maslen SL, Skehel JM, Komander D (2018) Mechanism of parkin activation by PINK1. *Nature* 559:410–414. <https://doi.org/10.1038/s41586-018-0224-x>
25. Goldberg MS, Fleming SM, Palacino JJ, Cepeda C, Lam HA, Bhatnagar A et al (2003) Parkin-deficient mice exhibit nigrostriatal deficits but not loss of dopaminergic neurons. *J Biol Chem* 278:43628–43635. <https://doi.org/10.1074/jbc.M308947200>
26. Gong G, Song M, Csordas G, Kelly DP, Matkovich SJ, Dorn GW 2nd (2015) Parkin-mediated mitophagy directs perinatal cardiac metabolic maturation in mice. *Science* 350:aad2459. <https://doi.org/10.1126/science.aad2459>
27. Gouider-Khouja N, Larnaout A, Amouri R, Sfar S, Belal S, Ben Hamida C et al (2003) Autosomal recessive parkinsonism linked to parkin gene in a Tunisian family. Clinical, genetic and pathological study. *Parkinsonism Relat Disord* 9:247–251. [https://doi.org/10.1016/s1353-8020\(03\)00016-6](https://doi.org/10.1016/s1353-8020(03)00016-6)
28. Gu WJ, Corti O, Araujo F, Hampe C, Jacquier S, Lucking CB et al (2003) The C289G and C418R missense mutations cause rapid sequestration of human Parkin into insoluble aggregates. *Neurobiol Dis* 14:357–364
29. Hampe C, Ardila-Osorio H, Fournier M, Brice A, Corti O (2006) Biochemical analysis of Parkinson's disease-causing variants of Parkin, an E3 ubiquitin-protein ligase with monoubiquitylation capacity. *Hum Mol Genet* 15:2059–2075. <https://doi.org/10.1093/hmg/ddl131>
30. Hayashi S, Wakabayashi K, Ishikawa A, Nagai H, Saito M, Maruyama M et al (2000) An autopsy case of autosomal-recessive juvenile parkinsonism with a homozygous exon 4 deletion in the parkin gene. *Mov Disord* 15:884–888
31. Hristova VA, Beasley SA, Rylett RJ, Shaw GS (2009) Identification of a novel Zn²⁺-binding domain in the autosomal recessive juvenile Parkinson-related E3 ligase parkin. *J Biol Chem* 284:14978–14986. <https://doi.org/10.1074/jbc.M808700200>
32. Hyun DH, Lee M, Hattori N, Kubo S, Mizuno Y, Halliwell B et al (2002) Effect of wild-type or mutant Parkin on oxidative damage, nitric oxide, antioxidant defenses, and the proteasome. *J Biol Chem* 277:28572–28577. <https://doi.org/10.1074/jbc.M20066200>
33. International Parkinson Disease Genomics C, Nalls MA, Plagnol V, Hernandez DG, Sharma M, Sheerin UM, Saad M et al (2011) Imputation of sequence variants for identification of genetic risks for Parkinson's disease: a meta-analysis of genome-wide association studies. *Lancet* 377:641–649. [https://doi.org/10.1016/S0140-6736\(10\)62345-8](https://doi.org/10.1016/S0140-6736(10)62345-8)
34. Itier JM, Ibanez P, Mena MA, Abbas N, Cohen-Salmon C, Bohme GA et al (2003) Parkin gene inactivation alters behaviour and dopamine neurotransmission in the mouse. *Hum Mol Genet* 12:2277–2291. <https://doi.org/10.1093/hmg/ddg239>
35. Jiang H, Ren Y, Yuen EY, Zhong P, Ghaedi M, Hu Z et al (2012) Parkin controls dopamine utilization in human midbrain dopaminergic neurons derived from induced pluripotent stem cells. *Nat Commun* 3:668. <https://doi.org/10.1038/ncomms1669>
36. Jiang H, Ren Y, Zhao J, Feng J (2004) Parkin protects human dopaminergic neuroblastoma cells against dopamine-induced apoptosis. *Hum Mol Genet* 13:1745–1754. <https://doi.org/10.1093/hmg/ddh180>
37. Jordan GM, Yoshioka S, Terao T (1994) The aggregation of bovine serum albumin in solution and in the solid state. *J Pharm Pharmacol* 46:182–185. <https://doi.org/10.1111/j.2042-7158.1994.tb03774.x>
38. Kano M, Takanashi M, Oyama G, Yoritaka A, Hatano T, Shiba-Fukushima K et al (2020) Reduced astrocytic reactivity in human brains and midbrain organoids with PRKN mutations. *NPJ Parkinsons Dis* 6:33. <https://doi.org/10.1038/s41531-020-00137-8>
39. Kasten M, Hartmann C, Hampf J, Schaake S, Westenberger A, Vollstedt EJ et al (2018) Genotype-phenotype relations for the Parkinson's disease genes parkin, PINK1, DJ1: MDSGene systematic review. *Mov Disord* 33:730–741. <https://doi.org/10.1002/mds.27352>
40. Khan NL, Graham E, Critchley P, Schrag AE, Wood NW, Lees AJ et al (2003) Parkin disease: a phenotypic study of a large case series. *Brain* 126:1279–1292. <https://doi.org/10.1093/brain/awg142>
41. Kiss R, Zhu M, Jojart B, Czajlik A, Solti K, Forizs B et al (2017) Structural features of human DJ-1 in distinct Cys106 oxidative states and their relevance to its loss of function in disease. *Biochim Biophys Acta Gen Subj* 1861:2619–2629. <https://doi.org/10.1016/j.bbagen.2017.08.017>
42. Kitada T, Asakawa S, Hattori N, Matsumine H, Yamamura Y, Minoishi S et al (1998) Mutations in the parkin gene cause autosomal recessive juvenile parkinsonism. *Nature* 392:605–608. <https://doi.org/10.1038/33416>
43. Kitada T, Pisani A, Karouani M, Haburcak M, Martella G, Tschertner A et al (2009) Impaired dopamine release and synaptic plasticity in the striatum of parkin^{-/-} mice. *J Neurochem* 110:613–621. <https://doi.org/10.1111/j.1471-4159.2009.06152.x>
44. Kitada T, Tomlinson JJ, Ao HS, Grimes DA, Schlossmacher MG (2012) Considerations regarding the etiology and future treatment of autosomal recessive versus idiopathic Parkinson disease.


- Curr Treat Options Neurol 14:230–240. <https://doi.org/10.1007/s11940-012-0175-8>
45. Klein C, Lohmann K (2009) Parkinson disease(s): is “Parkin disease” a distinct clinical entity? *Neurology* 72:106–107. <https://doi.org/10.1212/01.wnl.0000333666.65522.8d>
 46. Koyano F, Okatsu K, Kosako H, Tamura Y, Go E, Kimura M, Kimura et al (2014) Ubiquitin is phosphorylated by PINK1 to activate parkin. *Nature* 510:162–166. <https://doi.org/10.1038/nature13392>
 47. Krezel A, Maret W (2016) The biological inorganic chemistry of zinc ions. *Arch Biochem Biophys* 611:3–19. <https://doi.org/10.1016/j.abb.2016.04.010>
 48. Kuhlmann T, Ludwin S, Prat A, Antel J, Bruck W, Lassmann H (2017) An updated histological classification system for multiple sclerosis lesions. *Acta Neuropathol* 133:13–24. <https://doi.org/10.1007/s00401-016-1653-y>
 49. Kumar A, Aguirre JD, Condos TE, Martinez-Torres RJ, Chaugule VK, Toth R et al (2015) Disruption of the autoinhibited state primes the E3 ligase parkin for activation and catalysis. *EMBO J* 34:2506–2521. <https://doi.org/10.15252/embj.201592337>
 50. LaVoie MJ, Cortese GP, Ostaszewski BL, Schlossmacher MG (2007) The effects of oxidative stress on parkin and other E3 ligases. *J Neurochem* 103:2354–2368. <https://doi.org/10.1111/j.1471-4159.2007.04911.x>
 51. LaVoie MJ, Ostaszewski BL, Weihofen A, Schlossmacher MG, Selkoe DJ (2005) Dopamine covalently modifies and functionally inactivates parkin. *Nat Med* 11:1214–1221. <https://doi.org/10.1038/nm1314>
 52. Lee SJ, Kim DG, Lee KY, Koo JS, Lee BJ (2018) Regulatory mechanisms of thiol-based redox sensors: lessons learned from structural studies on prokaryotic redox sensors. *Arch Pharm Res* 41:583–593. <https://doi.org/10.1007/s12272-018-1036-0>
 53. Lesage S, Lunati A, Houot M, Romdhan SB, Clot F, Tesson C, French Parkinson Disease Genetics Study G et al (2020) Characterization of recessive Parkinson disease in a large multicenter study. *Ann Neurol* 88:843–850. <https://doi.org/10.1002/ana.25787>
 54. Liguori I, Russo G, Curcio F, Bulli G, Aran L, Della-Morte D et al (2018) Oxidative stress, aging, and diseases. *Clin Interv Aging* 13:757–772. <https://doi.org/10.2147/CIA.S158513>
 55. Lucking CB, Durr A, Bonifati V, Vaughan J, De Michele G, Gasser T et al (2000) Association between early-onset Parkinson’s disease and mutations in the parkin gene. *N Engl J Med* 342:1560–1567. <https://doi.org/10.1056/NEJM200005253422103>
 56. Maret W (2006) Zinc coordination environments in proteins as redox sensors and signal transducers. *Antioxid Redox Signal* 8:1419–1441. <https://doi.org/10.1089/ars.2006.8.1419>
 57. Matheoud D, Sugiura A, Bellemare-Pelletier A, Laplante A, Rondeau C, Chemali M, Fazel A et al (2016) Parkinson’s disease-related proteins PINK1 and parkin repress mitochondrial antigen presentation. *Cell* 166:314–327. <https://doi.org/10.1016/j.cell.2016.05.039>
 58. Matsuda N, Sato S, Shiba K, Okatsu K, Saisho K, Gautier CA et al (2010) PINK1 stabilized by mitochondrial depolarization recruits Parkin to damaged mitochondria and activates latent Parkin for mitophagy. *J Cell Biol* 189:211–221. <https://doi.org/10.1083/jcb.200910140>
 59. McLelland GL, Soubannier V, Chen CX, McBride HM, Fon EA (2014) Parkin and PINK1 function in a vesicular trafficking pathway regulating mitochondrial quality control. *EMBO J* 33:282–295. <https://doi.org/10.1002/embj.201385902>
 60. Meng F, Yao D, Shi Y, Kabakoff J, Wu W, Reicher J et al (2011) Oxidation of the cysteine-rich regions of parkin perturbs its E3 ligase activity and contributes to protein aggregation. *Mol Neurodegener* 6:34. <https://doi.org/10.1186/1750-1326-6-34>
 61. Micsonai A, Wien F, Bulyaki E, Kun J, Moussong E, Lee YH et al (2018) BeStSel: a web server for accurate protein secondary structure prediction and fold recognition from the circular dichroism spectra. *Nucleic Acids Res* 46:W315–W322. <https://doi.org/10.1093/nar/gky497>
 62. Micsonai A, Wien F, Keryna L, Lee YH, Goto Y, Refregiers M et al (2015) Accurate secondary structure prediction and fold recognition for circular dichroism spectroscopy. *Proc Natl Acad Sci USA* 112:E3095–3103. <https://doi.org/10.1073/pnas.1500851112>
 63. Mouton-Liger F, Rosazza T, Sepulveda-Diaz J, Jeang A, Hassoun SM, Claire E et al (2018) Parkin deficiency modulates NLRP3 inflammasome activation by attenuating an A20-dependent negative feedback loop. *Glia* 66:1736–1751. <https://doi.org/10.1002/glia.23337>
 64. Muller CH, Lee TK, Montano MA (2013) Improved chemiluminescence assay for measuring antioxidant capacity of seminal plasma. *Methods Mol Biol* 927:363–376. https://doi.org/10.1007/978-1-62703-038-0_31
 65. Muller-Rischart AK, Pils A, Beaudette P, Patra M, Hadian K, Funke M et al (2013) The E3 ligase parkin maintains mitochondrial integrity by increasing linear ubiquitination of NEMO. *Mol Cell* 49:908–921. <https://doi.org/10.1016/j.molcel.2013.01.036>
 66. Nalls MA, Pankratz N, Lill CM, Do CB, Hernandez DG, Saad M, International Parkinson’s Disease Genomics C, Parkinson’s Study Group Parkinson’s Research: The Organized GI, andMe, GenePd, NeuroGenetics Research C, Hussman Institute of Human G, Ashkenazi Jewish Dataset I, Cohorts for H, Aging Research in Genetic E, North American Brain Expression C, United Kingdom Brain Expression C, Greek Parkinson’s Disease C, Alzheimer Genetic Analysis G et al (2014) Large-scale meta-analysis of genome-wide association data identifies six new risk loci for Parkinson’s disease. *Nat Genet* 46:989–993. <https://doi.org/10.1038/ng.3043>
 67. Narendra DP, Jin SM, Tanaka A, Suen DF, Gautier CA, Shen J et al (2010) PINK1 is selectively stabilized on impaired mitochondria to activate Parkin. *PLoS Biol* 8:e1000298. <https://doi.org/10.1371/journal.pbio.1000298>
 68. Okarmus J, Bogetofte H, Schmidt SI, Ryding M, Garcia-Lopez S, Ryan BJ et al (2020) Lysosomal perturbations in human dopaminergic neurons derived from induced pluripotent stem cells with PARK2 mutation. *Sci Rep* 10:10278. <https://doi.org/10.1038/s41598-020-67091-6>
 69. Ozawa K, Komatsubara AT, Nishimura Y, Sawada T, Kawafune H, Tsumoto H et al (2013) S-nitrosylation regulates mitochondrial quality control via activation of parkin. *Sci Rep* 3:2202. <https://doi.org/10.1038/srep02202>
 70. Palacino JJ, Sagi D, Goldberg MS, Krauss S, Motz C, Wacker M et al (2004) Mitochondrial dysfunction and oxidative damage in parkin-deficient mice. *J Biol Chem* 279:18614–18622. <https://doi.org/10.1074/jbc.M401135200>
 71. Panicker N, Dawson VL, Dawson TM (2017) Activation mechanisms of the E3 ubiquitin ligase parkin. *Biochem J* 474:3075–3086. <https://doi.org/10.1042/BCJ20170476>
 72. Paris G, Kraszewski S, Ramseyer C, Enescu M (2012) About the structural role of disulfide bridges in serum albumins: evidence from protein simulated unfolding. *Biopolymers* 97:889–898. <https://doi.org/10.1002/bip.22096>
 73. Pawlyk AC, Giasson BI, Sampathu DM, Perez FA, Lim KL, Dawson VL et al (2003) Novel monoclonal antibodies demonstrate biochemical variation of brain parkin with age. *J Biol Chem* 278:48120–48128. <https://doi.org/10.1074/jbc.M306889200>

74. Periquet M, Corti O, Jacquier S, Brice A (2005) Proteomic analysis of parkin knockout mice: alterations in energy metabolism, protein handling and synaptic function. *J Neurochem* 95:1259–1276. <https://doi.org/10.1111/j.1471-4159.2005.03442.x>
75. Pickrell AM, Huang CH, Kennedy SR, Ordureau A, Sideris DP, Hoekstra JG et al (2015) Endogenous Parkin preserves dopaminergic substantia nigral neurons following mitochondrial DNA mutagenic stress. *Neuron* 87:371–381. <https://doi.org/10.1016/j.neuron.2015.06.034>
76. Polman CH, Reingold SC, Banwell B, Clanet M, Cohen JA, Filippi M et al (2011) Diagnostic criteria for multiple sclerosis: 2010 revisions to the McDonald criteria. *Ann Neurol* 69:292–302. <https://doi.org/10.1002/ana.22366>
77. Pramstaller PP, Schlossmacher MG, Jacques TS, Scaravilli F, Eskelson C, Pepivani I et al (2005) Lewy body Parkinson's disease in a large pedigree with 77 Parkin mutation carriers. *Ann Neurol* 58:411–422. <https://doi.org/10.1002/ana.20587>
78. Ratan RR (1999) Antioxidants and the treatment of neurological disease. In: Koliatsos VE, Ratan, RR (ed) *Cell death and diseases of the nervous system*. Humana Press, Totowa. https://doi.org/10.1007/978-1-4612-1602-5_32
79. Rodriguez-Navarro JA, Casarejos MJ, Menendez J, Solano RM, Rodal I, Gomez A et al (2007) Mortality, oxidative stress and tau accumulation during ageing in parkin null mice. *J Neurochem* 103:98–114. <https://doi.org/10.1111/j.1471-4159.2007.04762.x>
80. Rosen KM, Veereshwarayya V, Moussa CE, Fu Q, Goldberg MS, Schlossmacher MG et al (2006) Parkin protects against mitochondrial toxins and beta-amyloid accumulation in skeletal muscle cells. *J Biol Chem* 281:12809–12816. <https://doi.org/10.1074/jbc.M512649200>
81. Schlossmacher MG, Frosch MP, Gai WP, Medina M, Sharma N, Forno L et al (2002) Parkin localizes to the Lewy bodies of Parkinson disease and dementia with Lewy bodies. *Am J Pathol* 160:1655–1667. [https://doi.org/10.1016/S0002-9440\(10\)61113-3](https://doi.org/10.1016/S0002-9440(10)61113-3)
82. Schlossmacher MG, Shimura H (2005) Parkinson's disease: assays for the ubiquitin ligase activity of neural Parkin. *Methods Mol Biol* 301:351–369
83. Segura-Aguilar J, Paris I, Munoz P, Ferrari E, Zecca L, Zucca FA (2014) Protective and toxic roles of dopamine in Parkinson's disease. *J Neurochem* 129:898–915. <https://doi.org/10.1111/jnc.12686>
84. Shevchenko A, Tomas H, Havlis J, Olsen JV, Mann M (2006) In-gel digestion for mass spectrometric characterization of proteins and proteomes. *Nat Protoc* 1:2856–2860. <https://doi.org/10.1038/nprot.2006.468>
85. Shimura H, Hattori N, Kubo S, Yoshikawa M, Kitada T, Matsumine H et al (1999) Immunohistochemical and subcellular localization of Parkin protein: absence of protein in autosomal recessive juvenile parkinsonism patients. *Ann Neurol* 45:668–672. [https://doi.org/10.1002/1531-8249\(199905\)45:5%3c668::aid-ana19%3e3.0.co;2-z](https://doi.org/10.1002/1531-8249(199905)45:5%3c668::aid-ana19%3e3.0.co;2-z)
86. Shin JH, Ko HS, Kang H, Lee Y, Lee YI, Pletinkova O et al (2011) PARIS (ZNF746) repression of PGC-1alpha contributes to neurodegeneration in Parkinson's disease. *Cell* 144:689–702. <https://doi.org/10.1016/j.cell.2011.02.010>
87. Shutinoski B, Hakimi M, Harmsen IE, Lunn M, Rocha J, Lengacher N et al (2019) Lrrk2 alleles modulate inflammation during microbial infection of mice in a sex-dependent manner. *Sci Transl Med*. <https://doi.org/10.1126/scitranslmed.aas9292>
88. Sliter DA, Martinez J, Hao L, Chen X, Sun N, Fischer TD et al (2018) Parkin and PINK1 mitigate STING-induced inflammation. *Nature* 561:258–262. <https://doi.org/10.1038/s41586-018-0448-9>
89. Solano RM, Casarejos MJ, Menendez-Cuervo J, Rodriguez-Navarro JA, Garcia de Yébenes J, Mena MA (2008) Glial dysfunction in parkin null mice: effects of aging. *J Neurosci* 28:598–611. <https://doi.org/10.1523/JNEUROSCI.4609-07.2008>
90. Solti K, Kuan WL, Forizs B, Kustos G, Mihaly J, Varga Z et al (2020) DJ-1 can form beta-sheet structured aggregates that co-localize with pathological amyloid deposits. *Neurobiol Dis* 134:104629. <https://doi.org/10.1016/j.nbd.2019.104629>
91. Spratt DE, Martinez-Torres RJ, Noh YJ, Mercier P, Manczyk N, Barber KR et al (2013) A molecular explanation for the recessive nature of parkin-linked Parkinson's disease. *Nat Commun* 4:1983. <https://doi.org/10.1038/ncomms2983>
92. Sriram SR, Li X, Ko HS, Chung KK, Wong E, Lim KL et al (2005) Familial-associated mutations differentially disrupt the solubility, localization, binding and ubiquitination properties of parkin. *Hum Mol Genet* 14:2571–2586. <https://doi.org/10.1093/hmg/ddi292>
93. Sun Y, Li H (2013) Functional characterization of SAG/RBX2/ROC2/RNF7, an antioxidant protein and an E3 ubiquitin ligase. *Protein Cell* 4:103–116. <https://doi.org/10.1007/s13238-012-2105-7>
94. Sun Y, Tan M, Duan H, Swaroop M (2001) SAG/ROC/Rbx/Hrt, a zinc RING finger gene family: molecular cloning, biochemical properties, and biological functions. *Antioxid Redox Signal* 3:635–650. <https://doi.org/10.1089/15230860152542989>
95. Takahashi H, Ohama E, Suzuki S, Horikawa Y, Ishikawa A, Morita T et al (1994) Familial juvenile parkinsonism: clinical and pathologic study in a family. *Neurology* 44:437–441. https://doi.org/10.1212/wnl.44.3_part_1.437
96. Unger T, Jacobovitch Y, Dantes A, Bernheim R, Peleg Y (2010) Applications of the Restriction Free (RF) cloning procedure for molecular manipulations and protein expression. *J Struct Biol* 172:34–44. <https://doi.org/10.1016/j.jsb.2010.06.016>
97. Vandiver MS, Paul BD, Xu R, Karuppagounder S, Rao F, Snowman AM et al (2013) Sulfhydration mediates neuroprotective actions of parkin. *Nat Commun* 4:1626. <https://doi.org/10.1038/ncomms2623>
98. Wang C, Ko HS, Thomas B, Tsang F, Chew KC, Tay SP et al (2005) Stress-induced alterations in parkin solubility promote parkin aggregation and compromise parkin's protective function. *Hum Mol Genet* 14:3885–3897. <https://doi.org/10.1093/hmg/ddi413>
99. Wang C, Tan JM, Ho MW, Zaiden N, Wong SH, Chew CL et al (2005) Alterations in the solubility and intracellular localization of parkin by several familial Parkinson's disease-linked point mutations. *J Neurochem* 93:422–431. <https://doi.org/10.1111/j.1471-4159.2005.03023.x>
100. Wang YQ, Tang BS, Yu RL, Li K, Liu ZH, Xu Q et al (2014) Association analysis of STK39, MCCC1/LAMP3 and sporadic PD in the Chinese Han population. *Neurosci Lett* 566:206–209. <https://doi.org/10.1016/j.neulet.2014.03.007>
101. Wauer T, Komander D (2013) Structure of the human Parkin ligase domain in an autoinhibited state. *EMBO J* 32:2099–2112. <https://doi.org/10.1038/emboj.2013.125>
102. Whitworth AJ, Theodore DA, Greene JC, Beneš H, Wes PD, Pallanck LJ (2005) Increased glutathione S-transferase activity rescues dopaminergic neuron loss in a Drosophila model of Parkinson's disease. *Proc Natl Acad Sci* 102:8024–8029. <https://doi.org/10.1073/pnas.0501078102>
103. Winklhofer KF, Henn IH, Kay-Jackson PC, Heller U, Tatzelt J (2003) Inactivation of parkin by oxidative stress and C-terminal truncations: a protective role of molecular chaperones. *J Biol Chem* 278:47199–47208. <https://doi.org/10.1074/jbc.M306769200>
104. Wong ES, Tan JM, Wang C, Zhang Z, Tay SP, Zaiden N et al (2007) Relative sensitivity of parkin and other cysteine-containing enzymes to stress-induced solubility alterations. *J Biol Chem* 282:12310–12318. <https://doi.org/10.1074/jbc.M609466200>

105. Xiao H, Jedrychowski MP, Schweppe DK, Huttlin EL, Yu Q, Heppner DE et al (2020) A quantitative tissue-specific landscape of protein redox regulation during aging. *Cell* 180(968–983):e924. <https://doi.org/10.1016/j.cell.2020.02.012>
106. Yamamura Y, Kuzuhara S, Kondo K, Yanagi T, Uchida M, Matsumine H et al (1998) Clinical, pathologic and genetic studies on autosomal recessive early-onset parkinsonism with diurnal fluctuation. *Parkinsonism Relat Disord* 4:65–72. [https://doi.org/10.1016/s1353-8020\(98\)00015-7](https://doi.org/10.1016/s1353-8020(98)00015-7)
107. Yao D, Gu Z, Nakamura T, Shi ZQ, Ma Y, Gaston B et al (2004) Nitrosative stress linked to sporadic Parkinson's disease: S-nitrosylation of parkin regulates its E3 ubiquitin ligase activity. *Proc Natl Acad Sci USA* 101:10810–10814. <https://doi.org/10.1073/pnas.0404161101>
108. Yi W, MacDougall EJ, Tang MY, Krahn AI, Gan-Or Z, Trempe JF et al (2019) The landscape of Parkin variants reveals pathogenic mechanisms and therapeutic targets in Parkinson's disease. *Hum Mol Genet* 28:2811–2825. <https://doi.org/10.1093/hmg/ddz080>
109. Yokochi M, Narabayashi H, Iizuka R, Nagatsu T (1984) Juvenile parkinsonism—some clinical, pharmacological, and neuropathological aspects. *Adv Neurol* 40:407–413
110. Zucca FA, Basso E, Cupaioli FA, Ferrari E, Sulzer D, Casella L et al (2014) Neuromelanin of the human substantia nigra: an update. *Neurotox Res* 25:13–23. <https://doi.org/10.1007/s12640-013-9435-y>
111. Zucca FA, Vanna R, Cupaioli FA, Bellei C, De Palma A, Di Silvestre D et al (2018) Neuromelanin organelles are specialized autolysosomes that accumulate undegraded proteins and lipids in aging human brain and are likely involved in Parkinson's disease. *NPJ Parkinsons Dis* 4:17. <https://doi.org/10.1038/s41531-018-0050-8>

Publisher's Note Springer Nature remains neutral with regard to jurisdictional claims in published maps and institutional affiliations.

Authors and Affiliations

Jacqueline M. Tokarew^{1,2} · Daniel N. El-Kodsi^{1,2} · Nathalie A. Lengacher^{1,2} · Travis K. Fehr^{1,2} · Angela P. Nguyen¹ · Bojan Shutinoski¹ · Brian O'Nuallain³ · Ming Jin³ · Jasmine M. Khan¹ · Andy C. H. Ng¹ · Juan Li¹ · Qiubo Jiang¹ · Mei Zhang⁴ · Liqun Wang³ · Rajib Sengupta^{5,6} · Kathryn R. Barber⁷ · An Tran⁷ · Doo Soon Im^{20,21} · Steve Callaghan²⁰ · David S. Park^{20,21} · Stephanie Zandee⁸ · Xiajun Dong⁹ · Clemens R. Scherzer⁹ · Alexandre Prat⁸ · Eve C. Tsai^{1,10} · Masashi Takanashi¹¹ · Nobutaka Hattori¹¹ · Jennifer A. Chan¹² · Luigi Zecca¹³ · Andrew B. West^{14,15} · Arne Holmgren⁵ · Lawrence Puente¹⁶ · Gary S. Shaw⁷ · Gergely Toth¹⁷ · John M. Woulfe^{1,4} · Peggy Taylor³ · Julianna J. Tomlinson^{1,18} · Michael G. Schlossmacher^{1,18,19} 

✉ Julianna J. Tomlinson
jtomlinson@ohri.ca

✉ Michael G. Schlossmacher
mschlossmacher@toh.ca

¹ Program in Neuroscience, Ottawa Hospital Research Institute, Ottawa, ON, Canada

² Graduate Program in Cellular and Molecular Medicine (Neuroscience), Faculty of Medicine, University of Ottawa, Ottawa, ON, Canada

³ BioLegend Inc., Dedham, MA, USA

⁴ Department of Pathology and Laboratory Medicine, The Ottawa Hospital, Ottawa, ON, Canada

⁵ Department of Biochemistry, Karolinska Institute, Stockholm, Sweden

⁶ Present Address: Amity Institute of Biotechnology, Amity University, Kolkata, West Bengal 700135, India

⁷ Department of Biochemistry, University of Western Ontario, London, ON, Canada

⁸ Department of Neuroscience, Faculty of Medicine, University of Montreal, Montreal, QC, Canada

⁹ Ann Romney Center for Neurologic Diseases, Brigham and Women's Hospital, Boston, MA, USA

¹⁰ Division of Neurosurgery, Department of Surgery, The Ottawa Hospital, Ottawa, ON, Canada

¹¹ Department of Neurology, Juntendo University School of Medicine, Tokyo, Japan

¹² Department of Pathology and Laboratory Medicine, University of Calgary, Calgary, AB, Canada

¹³ Institute of Biomedical Technologies, Italian National Research Council, Segrate, Milan, Italy

¹⁴ Department of Neurobiology, Duke University, Durham, NC, USA

¹⁵ Department of Pharmacology and Cancer Biology, Duke University, Durham, NC, USA

¹⁶ Proteomics Core Facility, Ottawa Hospital Research Institute, Ottawa, ON, Canada

¹⁷ Institute of Organic Chemistry, Research Center for Natural Sciences, Budapest, Hungary

¹⁸ University of Ottawa Brain and Mind Research Institute, Ottawa, ON, Canada

¹⁹ Division of Neurology, Department of Medicine, The Ottawa Hospital, Ottawa, ON, Canada

²⁰ Department of Cellular and Molecular Medicine, University of Ottawa, Ottawa, ON, Canada

²¹ Present Address: Hotchkiss Brain Institute, University of Calgary, Calgary, AB, Canada